

RESEARCH ARTICLE

10.1002/2014JD021849

Key Points:

- In situ wind observations are used to assess the realism of (re)analyses
- Errors on UTLS winds can exceed 10 m/s for 10 consecutive days
- Misrepresented equatorial waves in poorly observed regions cause these errors

Correspondence to:

A. Podglajen,
apodgla@lmd.ens.fr

Citation:

Podglajen, A., A. Hertzog, R. Plougonven, and N. Žagar (2014), Assessment of the accuracy of (re)analyses in the equatorial lower stratosphere, *J. Geophys. Res. Atmos.*, 119, 11,166–11,188, doi:10.1002/2014JD021849.

Received 2 APR 2014

Accepted 26 AUG 2014

Accepted article online 1 SEP 2014

Published online 9 OCT 2014

Assessment of the accuracy of (re)analyses in the equatorial lower stratosphere

Aurélien Podglajen¹, Albert Hertzog¹, Riwal Plougonven¹, and Nedjeljka Žagar²

¹Laboratoire de Météorologie Dynamique, École Polytechnique, Palaiseau, France, ²Department of Physics, Faculty of Mathematics and Physics, University of Ljubljana, Ljubljana, Slovenia

Abstract The accuracy of horizontal winds and temperature in the equatorial lower stratosphere is evaluated in different (re)analyses (European Centre for Medium-Range Weather Forecasts (ECMWF) operational analysis, ERA Interim, and Modern-Era Retrospective Analysis for Research and Applications) using an independent data set collected at low latitudes during long-duration balloon flights in early 2010. The three analyzed wind products are found significantly less accurate than in the extratropics, with periods of ≥ 10 m/s disagreement with the observations lasting several days. To highlight the dynamical context in which the major disagreement events occur, case studies are carried out. The events are shown to be related to an improper representation of large-scale equatorial Kelvin and Yanai wave packets with vertical wavelengths smaller than 5 km. Such events can induce large errors on trajectories computed with analyzed winds relatively to the actual (balloon) trajectory: 4000 km separation after 5 days of calculation. Reasons for analyses inaccuracy are discussed. The vertical resolution of the underlying model likely plays a role, but the main factor responsible for deficiencies appears to be the lack of wind observations. Indeed, errors in analyzed winds during the campaign have a strong longitudinal structure, with root-mean-square errors twice as large over the Indian Ocean and western Pacific, poorly covered by radiosounding stations, as over the Maritime Continent or South America. For the ECMWF analysis, this structure mirrors that of the analysis increments, which have largest amplitudes over observed regions. We argue that the reported events are more likely to happen during maximum shear phases of the quasi-biennial oscillation.

1. Introduction

Dynamical and physical processes in the tropical tropopause layer (TTL) and equatorial lower stratosphere play key roles in the Earth's climate system, as they notably set the boundary conditions for air parcels that enter the middle atmosphere overworld [Fueglistaler *et al.*, 2009]. Such processes include cirrus cloud formation, dehydration, and transport of gaseous chemical species and aerosols to the stratosphere. Because they strongly depend on the history of air parcels, i.e., on the Lagrangian evolution of temperature, humidity, and diabatic heating, these processes are often investigated using trajectories calculated with (re)analysis products [e.g., Fueglistaler *et al.*, 2005; Reverdy *et al.*, 2012; Liu *et al.*, 2010]. In these studies, errors in the analyzed wind fields have been identified as a potential source of uncertainty in the results, and, for instance, Hasebe *et al.* [2013] reported on differences that can reach a few m/s between analyzed and observed winds in the TTL over the Maritime Continent. Yet it is generally difficult to provide a quantitative estimate of such errors at the global scale, as in situ observations of upper air winds are sparse in the tropics and most of the available measurements are assimilated by the operational centers.

In the equatorial upper troposphere-lower stratosphere (UTLS), the dynamics at planetary and synoptic scales is dominated by equatorial waves, which have been a subject of much research since their first analytical derivation by Matsuno [1966]. They have been identified in many data sets in the middle atmosphere, such as radiosoundings [Yanai and Maruyama, 1966], satellite observations of temperature [Ern *et al.*, 2008] and constituents, as well as operational analyses [Žagar *et al.*, 2009] and reanalyses [e.g., Lott *et al.*, 2009; Flannaghan and Fueglistaler, 2012, 2013]. Those studies have shown that large-scale Yanai and Kelvin waves have the largest amplitudes. The interest in equatorial waves comes among others from their major impact on physical processes in the tropical UTLS. By structuring temperature and wind shear, they influence the formation and life cycle of cirrus clouds [Boehm and Verlinde, 2000] and the subsequent dehydration [e.g., Dinh *et al.*, 2012; Suzuki *et al.*, 2013]. They also affect vertical transport of constituents by modifying the diabatic heating rates [Fueglistaler and Fu, 2006] and the efficiency of turbulent diffusivity (through changes

in wind shear and static stability). Last, large-scale equatorial waves bring an important contribution to the driving of the quasi-biennial oscillation (QBO), together with short-scale gravity waves [Kawatani *et al.*, 2010; Evan *et al.*, 2012].

Equatorial waves are primarily forced by the release of latent heat associated with tropospheric deep convection [Bergman and Salby, 1994; Horinouchi *et al.*, 2003; Ortlund *et al.*, 2011]. While convection itself can be organized in convectively coupled equatorial waves [Wheeler and Kiladis, 1999], stratospheric waves are free modes that vertically propagate away from the forcing regions. Because deep convection is parameterized in numerical models, the explicit generation of equatorial waves in the models is questionable, as is the accuracy of the associated propagating modes in the stratosphere. Therefore, the accurate representation of stratospheric equatorial waves in the analyses likely relies on the availability of tropical observations and on the assimilation methodology.

Now there are specific challenges associated with data assimilation for atmospheric analyses at low latitudes. In contrast with the extratropics, there does not exist a predominant balance between the mass and wind fields in the tropics [Žagar *et al.*, 2013]. As a consequence, the wealth of (indirect) temperature measurements provided by satellite observations is not as useful to constrain the winds as they are in the extratropics. As pointed out by Baker *et al.* [2013], the three-dimensional wind field is then the most important measurement needed to accurately assess the dynamics of the tropical atmosphere. However, wind information is particularly deficient in the tropics: in situ measurements are scarce and inhomogeneous, with most of the radiosounding stations located over the Maritime Continent and South America. Very wide regions (eastern Pacific, Indian Ocean) remain virtually void of any direct wind observations. In most of the troposphere, atmospheric motion vectors (AMVs) data represent an important source of wind observations, but in the UTLS the only regular information on winds is provided by radiosoundings. The model dynamics is thus probably less driven by the assimilation of observations in the equatorial UTLS than anywhere else at the same altitude, and large errors in the analyzed winds could result from this relative lack of observations.

In this context, the purpose of the present study is to provide some insights on the representation of the equatorial lower stratosphere dynamics in different (re)analyses and to investigate reasons for potential (re)analyses errors. To do so, we use measurements collected during the PreConcordiasi campaign of long-duration balloons drifting at 19–20 km within 10° of the equator. Long-duration stratospheric balloon campaigns [e.g., Hertzog *et al.*, 2007; Rabier *et al.*, 2010] provide in situ, high-resolution information on the dynamics and constitute a unique opportunity to evaluate the precision of trajectory calculations and process studies. In particular, the observations collected during the PreConcordiasi balloon flights were not assimilated by the forecasting systems that are assessed in this study. Such long-duration balloon observations have been previously used for similar purposes in the Southern Hemisphere tropics [Knudsen *et al.*, 2006] or over both northern and southern polar areas [Hertzog *et al.*, 2004; Boccara *et al.*, 2008].

The study is organized along the following structure. Section 2 presents both the observational and numerical data sets used in this work, as well as the methodology used to interpolate the analyses on the balloon positions. In section 3, we compare the analyses to the observations and provide global statistics as well as the time evolution of the analysis errors. We also point out specific time periods associated with larger discrepancies. In section 4, we focus more deeply on three of these time periods and try to identify the dynamical processes that are responsible for the observed differences between the observations and the analyses. Section 5 provides a discussion on the causes that may explain why models have difficulties to accurately simulate the atmospheric winds during these time periods. We also explore how frequently these events may occur, as well as the consequences on the accuracy of simulated trajectories. Finally, a summary and the conclusions are given in section 6.

2. Data Sets and Methodology of Comparison

2.1. Balloon Observations

To prepare for the Concordiasi campaign [Rabier *et al.*, 2010], the French Space Agency (Centre National d'Etudes Spatiales (CNES)) launched three superpressure balloons (SPBs) from Seychelles Islands (55.5°E, 4.6°N) in February 2010. SPBs are closed, spherical balloons filled with helium and are advected by the winds on isopycnic (constant density) surfaces [e.g., Massman, 1978]. Each of the three balloons carried a GPS providing its 3-D position and the TSEN (thermodynamical sensor) meteorological package that performs in situ observations of pressure and temperature every 30 s. The horizontal components of the wind are estimated

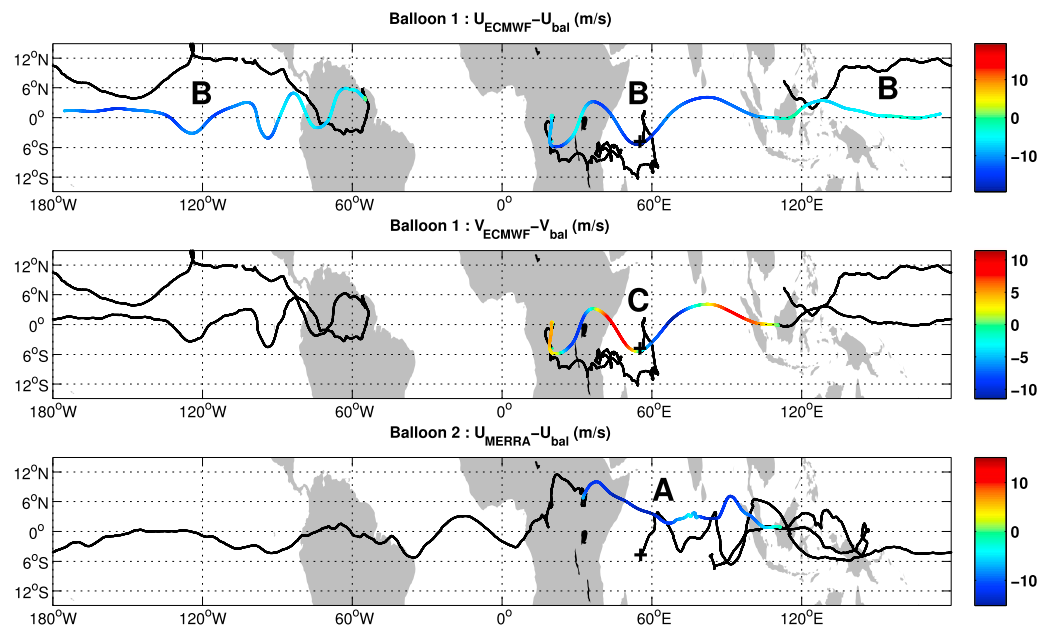


Figure 1. Trajectories of balloons 1 and 2. The colored part of the trajectories limit the geographic location of the case studies, designated by the letters A, B, and C. In addition, colors indicate differences between observed and analyzed fields: differences between (top) observations and ECMWF analysis zonal wind, (middle) observations and ECMWF analysis meridional wind, and (bottom) observations and MERRA zonal wind. The black crosses indicate the launching site, Seychelles Islands.

from the successive positions of the balloons, as determined every minute by the onboard GPS receiver. The TSEN temperature sensors (thermistors) are calibrated in the laboratory, while factory calibration is used for the pressure sensor (Paroscientific Model 6000-16B) (see below for more details regarding accuracy and precision of those sensors). As usually done during such balloon flights [Hertzog *et al.*, 2007], the temperature sensors were put at the lower end of the flight chain (the mechanical tether suspended below the balloon that links all the flight devices) in order to avoid any perturbation due to either the balloon or the gondolas. Additionally, the balloons carried two other lower accuracy thermistors aimed at monitoring the balloon characteristics (e.g., absence of leaks in the envelop) and located upper in the flight chain. These sensors are therefore more prone to errors, especially during daytime when the Sun heats the elements in the flight chain.

With an equilibrium density of about 0.1 kg/m^3 , the balloons flew between 55 and 65 hPa (19–20 km altitude). For each balloon the pressure stays within $\pm 3 \text{ hPa}$ of an average value, except during short (a few hours) depressurization events that represent a little fraction of the flight duration (less than 2%). The balloon trajectories are displayed in Figure 1. Two of them stayed within 15° from the equator for 3 months, but one drifted away into the Southern Hemisphere subtropical circulation (not shown). The present study focuses on the two balloons that continuously flew in the tropics and were therefore sampling the lower stratosphere equatorial dynamics. Figure 2 shows a Hovmöller diagram of the equatorial wind in the European Centre for Medium-Range Weather Forecasts (ECMWF) operational analyses, on a model level located near the balloon flight level. It provides some insights into the UTLS dynamics at the time of the flights. Balloon 1 longitude is superimposed in black in that figure. In particular, Figure 2 (left; zonal velocity) illustrates the zonal mean zonal velocity reversal in early April 2010 due to the phase change of the QBO at 60 hPa, as well as the eastward propagation of several planetary-scale Kelvin wave packets. The QBO phase change was experienced by the balloons, which first drifted eastward toward the Maritime Continent (except for some days at the beginning of the first flight) but switched to a westward drift at the end of the flights. Figure 2 (right; meridional velocity), on the other hand, highlights the eastward propagation of Yanai (or mixed Rossby-gravity) wave packets, with smaller scales than the Kelvin wave patterns.

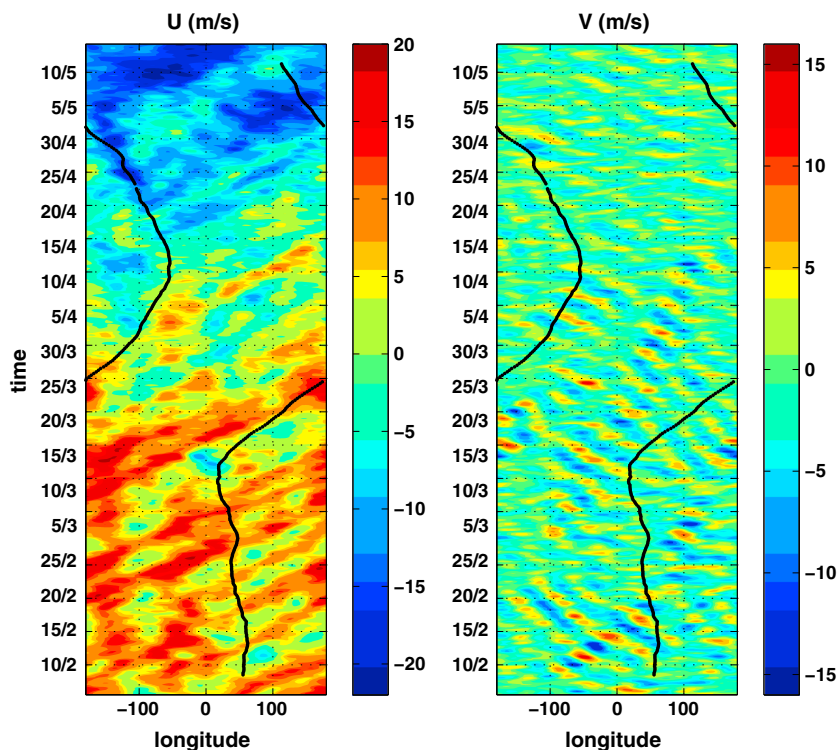


Figure 2. Hovmöller diagrams of (left) zonal and (right) meridional wind at the equator in ECMWF analysis, at the model level 32 (about 59 hPa). The longitude of balloon 1 every 6 h is figured by the black dots.

2.2. (Re)Analysis Products

In this study, the measurements from the PreConcordiasi campaign are compared to different (re)analyses data sets: the European Center for Medium-Range Weather Forecasts operational analysis (which will be referred to as ECMWF analysis), ERA Interim reanalysis (referred to as ERAi), and the NASA Modern-Era Retrospective Analysis for Research and Applications reanalysis (referred to as MERRA). Our purpose here is not to provide an extensive intercomparison of these (re)analyses but rather to assess their accuracy against observations in the equatorial lower stratosphere. Hence, our limited choice of analyses aims at (1) including a state-of-the-art operational analysis product, (2) including modern reanalyses, since trajectory studies are generally performed with reanalyses, and (3) having products from two distinct analysis centers to illustrate the uncertainty of reanalyses.

The ECMWF analyses are produced twice per day as a result of the operational 4-D variational (var) assimilation system and serve as initial state for the medium-range 10 day deterministic forecast. At the time of the PreConcordiasi campaign, the ECMWF atmospheric model (cycle 36r1) had a T1279 spectral truncation, which corresponds to a horizontal resolution of $0.125^\circ \times 0.125^\circ$. The model used 91 levels on the vertical, 10 of which located in the lower stratosphere (between 100 and 40 hPa).

We also compared the balloon observations to the ERAi reanalysis product [Dee *et al.*, 2011], which is commonly used for trajectory calculations in the TTL. One of the main differences with the operational analyses is a coarser horizontal (T255 truncation, ~ 79 km) and vertical resolution (60 levels), with in particular five levels in the lower stratosphere. ERAi furthermore uses an earlier version of the atmospheric forecast model (cycle 31r2), which was operational in early 2007. Both operational model and reanalysis system use a 4-D variational assimilation scheme with a 12 h assimilation window.

MERRA is provided by NASA and is based on version 5 of the Goddard Earth Observing System-5 atmospheric model and the associated 3-D var data assimilation system [Rienecker *et al.*, 2011]. The model is integrated in physical space, and outputs are available with a horizontal resolution of $2/3^\circ$ in longitude and 0.5° in latitude. The model has 72 levels between the surface and the top of the atmosphere (among which five are located in the lower stratosphere, between 100 and 40 hPa).

2.3. Comparisons and Uncertainties

To carry out the comparison between the analyses and the observations, we interpolated the analysis fields to the position and time of the balloon measurements. Whatever the analysis product, we used the 6-hourly archive (at 00, 06, 12, and 18 UTC) at full horizontal resolution and on model levels and did not make use of any 3 h intermediate forecast. The interpolation is performed with cubic splines in the three space dimensions, as well as in time. We used conventional latitude-longitude horizontal grid, and log-pressure as the vertical coordinate. Note that because model levels are hybrid sigma-pressure levels, we had to compute model-level pressure along the balloon trajectories before carrying out the vertical interpolation. For this vertical interpolation, we have used analyses of the four levels closest to the balloon.

While we aim here at characterizing the accuracy of the analysis products, differences between observations and the analyses could also stem from uncertainties in the observations and in the interpolation. Hence, we discuss these below.

Uncertainties in the observed winds are due to the limited precision of the GPS and to the balloon not being a perfect tracer of the atmospheric wind. For the PreConcordiasi campaign, the GPS precision on the balloon position causes a RMS noise 0.02 m/s in the derived horizontal velocities. The non-Lagrangian part of the balloon horizontal displacement accounts for another 0.05 m/s, based on an analysis of the various forces that act on the balloon [Vial *et al.*, 2001]. Combining the uncorrelated GPS uncertainties and the non-Lagrangian behavior of the balloon gives a typical uncertainty in wind observations of $\sigma_{w_{\text{obs}}} \approx 0.06$ m/s. Regarding temperature observations, appropriate calibration of the TSEN sensors in the laboratory ensures an accuracy of $\sigma_{T_{\text{obs}}} = 0.3$ K [Boccara *et al.*, 2008].

The interpolation of analysis fields along balloon trajectory is another source of differences due to the uncertainties in the balloon position and to the method of interpolation itself. Given the pressure sensor (absolute) accuracy of 10 Pa (i.e., about 10 m at the balloon flight level) and the strong vertical shears, the uncertainty in the balloon vertical position is by far the dominant source of error associated with the balloon position during the interpolation. With a vertical shear of at most 10 m/s between 60 and 54 hPa (≈ 14 m/s/km), we estimate an upper bound of this uncertainty to be about 0.15 m/s. On the other hand, the interpolation uncertainty is estimated to be of $\lesssim 0.8$ m/s by comparing different interpolation methods (linear, nearest). Thus, the additional error due to the interpolation process is $\sigma_{w_{\text{intrp}}} \approx 0.9$ m/s. In temperature, similar considerations suggest a typical error of $\sigma_{T_{\text{intrp}}} = 0.1$ K.

Both the observation and interpolation contributions are uncorrelated. The global uncertainty associated with those two factors therefore is $\sigma_w = \sqrt{\sigma_{w_{\text{obs}}}^2 + \sigma_{w_{\text{intrp}}}^2} \approx 0.9$ m/s in wind and $\sigma_T = \sqrt{\sigma_{T_{\text{obs}}}^2 + \sigma_{T_{\text{intrp}}}^2} \approx 0.3$ K in temperature. Any significantly larger difference between observations and (re)analyses can be interpreted as an analysis error. We note in advance that there is an order of magnitude between what error the above sources could produce and the observed differences. The latter includes phenomena that cannot be represented by the analysis because their time or spatial scales are too small compared to the model grid, i.e., the representativeness error. It also includes phenomena that in principle could be represented but are missing because of model deficiencies, deficiencies of data assimilation, and insufficient constraints from observations.

3. Estimation of (Re)Analysis Errors

We provide below statistics and space-time distribution of differences between balloon observations and interpolated fields from ECMWF operational analysis and MERRA reanalysis. For the sake of brevity and since winds for ERAI and the operational ECMWF analyses were found to be quite similar, we choose to perform a detailed analysis of the operational product only since it has a somewhat better average score. This does not necessarily imply that reasons behind similar score shown in Table B1 for ERAI and operational analyses are the same. Some results for the ERAI data set are presented in Appendix B.

3.1. Statistics of Analysis Errors

The first two PreConcordiasi balloons flew at similar altitudes (both between 19 and 20 km), and we present their statistics together. Regarding temperature measurements, we only use the second balloon because the TSEN temperature sensors were broken during the launch operations of the first balloon.

Figure 3 displays the histograms of analysis-observation differences in zonal and meridional winds, as well as in temperature. Starting with the meridional wind (middle), ECMWF and MERRA distributions both

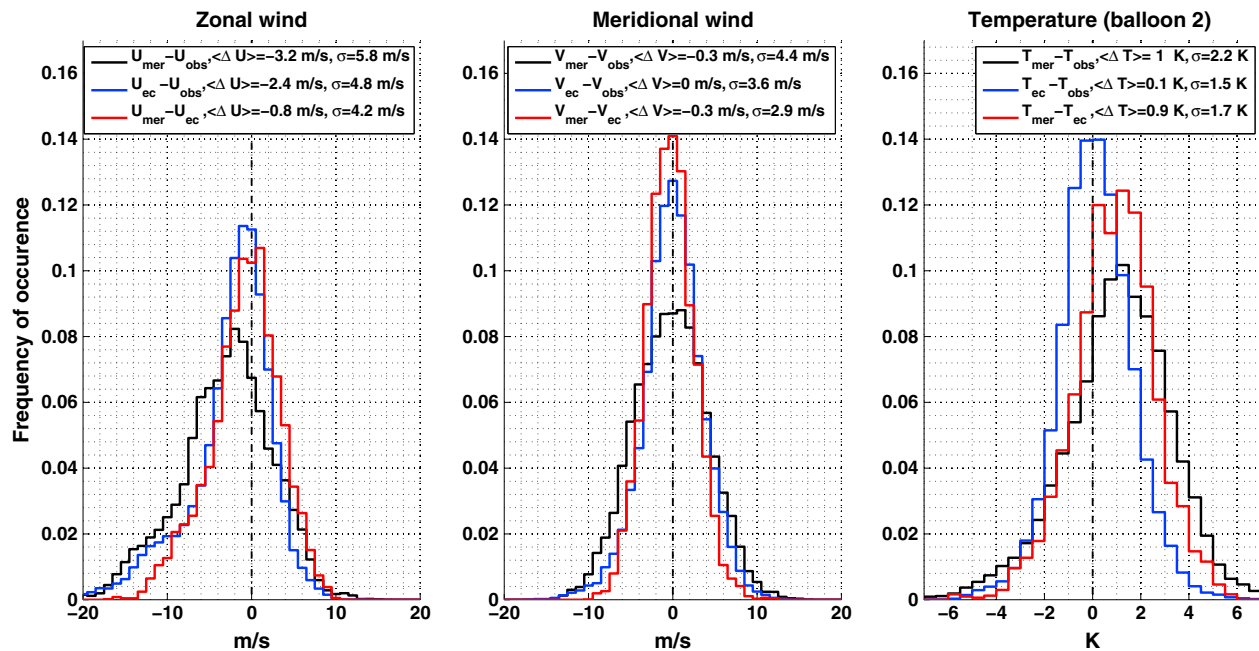


Figure 3. Distributions of differences between observations and analyses along balloon trajectories, for (left) zonal wind, (middle) meridional wind, and (right) balloon 2 temperature. Differences between MERRA and observations are in black and ECMWF and observations in blue. For comparison purposes, the distributions of differences between MERRA and ECMWF along balloons trajectories are figured in red.

approximately exhibit a centered Gaussian distribution, with a standard deviation of 3.6 and 4.4 m/s for ECMWF and MERRA, respectively. Errors larger in magnitude than 3.6 m/s typically occurred during one third of the flight duration.

The analyses are less accurate in representing the observed zonal winds (Figure 3, left) than the meridional ones. Indeed, the histograms display relatively large negative biases: -2.3 m/s for ECMWF operational analysis and -3.2 m/s for MERRA, and the associated distributions are no longer gaussian. They exhibit long tails toward negative values, corresponding to an underestimation of the observed zonal winds. For instance, errors more negative than -7 m/s occur 15% of the flight duration for ECMWF and 22% for MERRA. For both wind components, we note that, in general, ECMWF analysis and MERRA are closer to one another than to the observations, suggesting some variability missed by both.

Regarding temperature, ECMWF analysis along the trajectory of balloon 2 (Figure 3, right) are in fairly good agreement with the measurements, with a weak warm bias of 0.1 K and a standard deviation of 1.5 K. MERRA results are slightly less accurate; the reanalysis has a warm bias of 1 K and a standard deviation of 2.2 K. Short-scale gravity waves, which are poorly resolved in the models, typically induce disturbances

Table 1. Mean (Re)Analysis Error Statistics (Bias Δ and Standard Deviation σ) for MERRA Reanalysis, ECMWF Operational Analysis, and ERA Interim Reanalysis During the PreConcordiasi Campaign and for the ECMWF Analysis During Previous Similar Balloon Campaigns: HIBISCUS [Knudsen et al., 2006], Vorcore [Boccara et al., 2008], and Ecuador [Vial et al., 2001]

	u (m/s)		v (m/s)		T (K)	
	Δu	σ_u	Δv	σ_v	ΔT	σ_T
MERRA-observation (this study)	-3.2	5.8	-0.3	4.4	1.0	2.2
ECMWF-observation (this study)	-2.3	4.8	0.0	3.6	0.1	1.5
MERRA-ECMWF (this study)	-0.8	4.2	-0.3	2.9	0.9	1.7
ERA Interim-observation (this study)	-2.7	5.1	-0.1	3.8	0.6	1.8
HIBISCUS (southern tropics, 2004)	-0.4	3.1	0.0	3.5	-0.9	1.3
Vorcore (Antarctica, 2005)	0.1	2.4	0.0	2.4	-0.4	1.2
Ecuador (Deep tropics, 1998)	-2.4	~ 8	-0.7	~ 8	~ 1	~ 3

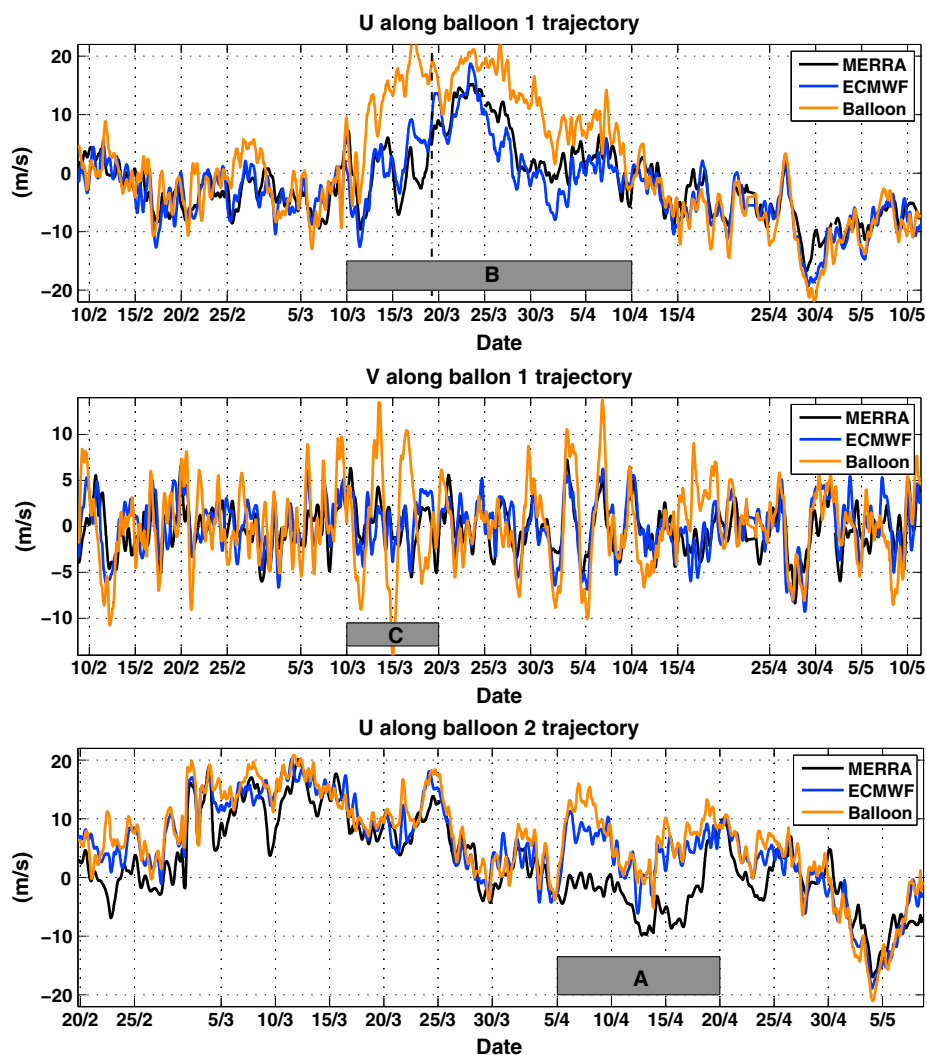


Figure 4. Time series of observed and analyzed winds (interpolated along the balloon trajectory). A 12 h moving average has been applied to highlight the long-standing disagreement events. The dotted line in the top row corresponds to the moment when the balloon crosses the longitude of Singapore (19/3).

with a RMS of 1 K in the PreConcordiasi observations and thus probably account for a large part of the analysis-observation standard deviations. Concerning the comparison between ECMWF and observations, it is recalled that the temperature measurements corresponding to the first balloon flight (for which ECMWF zonal wind errors are the largest) were not available to compute the statistics and might have somewhat degraded the reported agreement (see section 4.2). Contrary to what was seen in winds, we note that for temperature ECMWF analysis is closer to observations than to MERRA.

On top of a higher resolution and a more sophisticated (4-D var) assimilation model cycle, the better accuracy of the ECMWF analyses in temperature may also be due to a larger number of assimilated temperature observations in the tropical lower stratosphere than MERRA, such as those provided by the COSMIC GPS radio occultation system [Anthes *et al.*, 2008].

Table 1 summarizes the means and standard deviations of the differences between analyses and observations during the PreConcordiasi campaign, together with the same statistics for the ECMWF operational analysis during previous balloon campaigns: Ecuador (deep tropics, 1998 [Vial *et al.*, 2001]), HIBISCUS (Southern Hemisphere subtropics, 2002–2004 [Knudsen *et al.*, 2006]), and Vorcore (Antarctica, 2005 [Boccaro *et al.*, 2008]). As just noted, we observe a fairly good agreement between the observed and the analyzed temperatures, with ERAi providing intermediate statistics between those of ECMWF operational analyses and MERRA reanalyses. Still, we note that even though the differences between analyzed and observed

Table 2. Cases of Important Disagreement Between Analysis and Balloon Observations During the PreConcordiasi Campaign^a

Case	A	B	C
Balloon	2	1	1
Analysis	MERRA	MERRA and ECMWF	MERRA and ECMWF
Field	u and T	u (T?)	v
Time period	5–20 April	10 March to 10 April	10–20 March
Location	Eastern Africa-Indian Ocean	Indian Ocean-Eastern Pacific	Indian Ocean
Bias	−9.3 m/s and 1.4 K	−9 m/s (ECMWF)	0.0 m/s
RMS	9.5 m/s and 2.2 K	9.1 m/s (ECMWF)	6 m/s

^aRMS stands for root-mean square difference and is calculated as $\sqrt{\sum(x_{an} - x_{obs})^2}$.

temperatures may not seem large, such values can still induce significant differences in the associated water vapor saturation mixing ratio [e.g., *Schoeberl et al.*, 2012].

Regarding the meridional wind, ECMWF and MERRA moments have comparable values to those of the previous post-2000 campaigns, the standard deviations being slightly larger in PreConcordiasi. On the other hand, the comparison with the Ecuador campaign in 1998 shows an obvious improvement of the ECMWF analyses in the deep tropics, in agreement with the advancements in the model [*Bechtold et al.*, 2008]. The situation is less encouraging with the zonal wind statistics: although ECMWF operational analyses do show an improvement in the deep tropics since 1998, the average root-mean-square errors with respect to observations are much larger during PreConcordiasi than during the post-2000 extratropical campaigns. PreConcordiasi biases exceed 2 m/s, 3 times their value during extratropical campaigns, and the standard deviations (>4 m/s) are almost twice as important.

Such results could be surprising as models have continuously improved in the recent years, and their vertical and horizontal resolutions have increased by at least 30% since the previous campaigns. Yet significant errors in (re)analyzed winds in equatorial regions are not unexpected. As mentioned in section 1, assimilation of spaceborne refractivity and radiances (indirect temperature observations) provides few constraints to the tropical wind fields, even in the case of a perfect model *Žagar et al.* [2004]. The comparison between the Antarctic Vorcore and equatorial PreConcordiasi campaigns is particularly striking in this respect, as the wind statistics are better during Vorcore (almost no bias and a ~ 2 m/s standard deviation).

3.2. Temporal and Geographic Distribution of the Errors

Having shown that winds in the analyses can significantly deviate from the observations, we now investigate whether these errors appear randomly along the trajectories or if they are associated with misrepresented localized events. Figure 4 shows selected time series of observed and analyzed winds. Note that a 12 h running mean has been applied to the observed time series on this graphic to highlight low-frequency variability and restrict the observations to time scales accessible in the (re)analyses. Whereas analyzed and observed winds are in relatively good agreement during long periods (e.g., 10 April to 10 May for balloon 1 in zonal wind and the whole flight for balloon 2 in ECMWF analyses), we also observe conspicuous periods with errors larger than 5 m/s that persist for time periods longer than 10 days.

Three main episodes of disagreement between observed and analyzed winds occurred during the PreConcordiasi campaign. Two of them are associated with zonal winds: one affects only MERRA during April 2010 and is recorded by the second balloon (we will refer to it as case A) and the other one involves both (re)analyses and lasts from 10 March until 10 April during the first balloon flight (case B). Those two episodes of discrepancies in zonal wind correspond to an underestimation of the wind by the (re)analyses compared to observations (a westward bias). They have substantial and statistically significant amplitudes: the mean bias during those two periods is larger than -9 m/s. The third case (case C) corresponds to an oscillation of amplitude ~ 10 m/s in the meridional wind record of balloon 1 that is missed (or largely underestimated) by both (re)analyses. The three cases and their characteristics are summarized in Table 2.

The time series for temperature along the second balloon trajectory (not displayed) show that ECMWF temperature errors appear almost randomly distributed. The same comment stands for MERRA, except for a 5 day period included in case A (7–12 April) during which the reanalysis overestimates temperature by about 4 K, creating a 1.4 K bias for all case A.

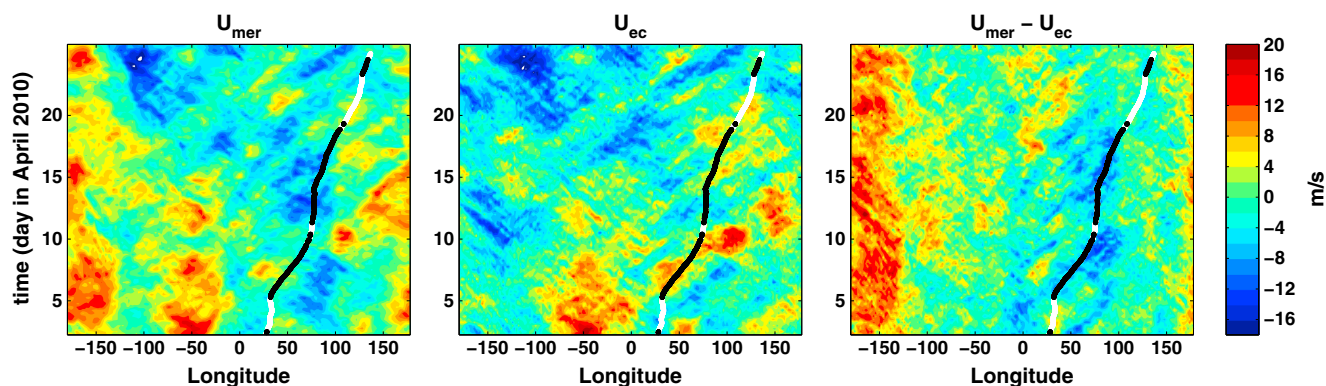


Figure 5. Hovmöller diagrams of zonal wind at the equator on level 61.5 hPa in (left) MERRA reanalysis, (middle) ECMWF operational analysis, and (right) the difference between the two. Balloon 2 trajectory is figured by the white-black line: the black color indicates time periods during which MERRA zonal wind error exceeds 8 m/s in magnitude.

The balloons sampled the whole equatorial belt, making it possible to consider the geographic repartition of the errors. Maps of differences along trajectories (see Figure 1) show that the three identified cases occurred over the Indian Ocean or Eastern Pacific. During case A, balloon 2 was drifting over western Africa and the Indian Ocean. Balloon 1 was at the same location during case C, while case B began over the Indian Ocean, then covered the Pacific and ended over South America. Despite the limited number of balloons during PreConcordiasi, there are thus hints of a geographical structure in the distribution of errors in the analyzed winds. This point will be further examined in section 5.

4. Case Studies of the Errors in Analyzed Winds

We investigate here the cases of strong disagreements pointed out in the previous section and summarized in Table 2. The two cases associated with large errors in the analyzed zonal winds (cases A and B) are investigated first. We then discuss case C, which had a clear signature in the meridional winds.

4.1. Case A

In contrast with MERRA reanalysis, ECMWF winds are close to the observations during this case (see Figure 4). For this reason, the information contained in the ECMWF analysis is used as the reference against which MERRA's fields are evaluated. To carry out the comparison between the two (re)analyses while taking into account the coarser MERRA resolution, we interpolated ECMWF and MERRA's fields on pressure levels close to MERRA model levels with the help of cubic splines in log-pressure coordinates. Horizontally, we simply used the analyzed fields without any interpolation on grid points common to both grids, every 2° in longitude and 1° in latitude. This horizontal resolution is indeed sufficient to study planetary-scale waves.

The difference during case A between MERRA reanalysis on the one hand and ECMWF analysis and the balloon observations on the other hand suggests that MERRA reanalysis misses a dynamical process with a strong signature in zonal wind. In the equatorial lower stratosphere, there are two obvious candidates: the QBO or equatorial waves. To discriminate between these processes, we display in Figure 5 Hovmöller diagrams of the zonal wind at the equator in MERRA (left), ECMWF analysis (middle), and the difference between ECMWF analysis and MERRA (right), on the 61.5 hPa level, i.e., close to balloon 2 flight level (64 hPa). Both data sets exhibit positive zonal wind anomalies propagating eastward, probably the signature of Kelvin waves. The most striking wave packet (with, however, a modulation of its amplitude) appears in ECMWF analysis from about 50° west on 1 April to the dateline on 15 April, i.e., with a ~20 m/s phase speed. Examination of the temperature field (not displayed) furthermore shows anomalies in quadrature with the zonal wind disturbances and with amplitudes consistent with upward propagating Kelvin wave packets. Between ~30° west and 100° east, the zonal wind difference between ECMWF and MERRA at the equator (Figure 5, right) is also structured in eastward propagating disturbances, with amplitudes up to 7–10 m/s, together with a stationary westward bias of about 4–5 m/s in MERRA zonal wind at the equator. We also note a positive bias in MERRA relatively to ECMWF in the central Pacific (around the dateline). Figure 5 therefore suggests that a lack of Kelvin wave packets over the Indian Ocean in MERRA is responsible for its reported

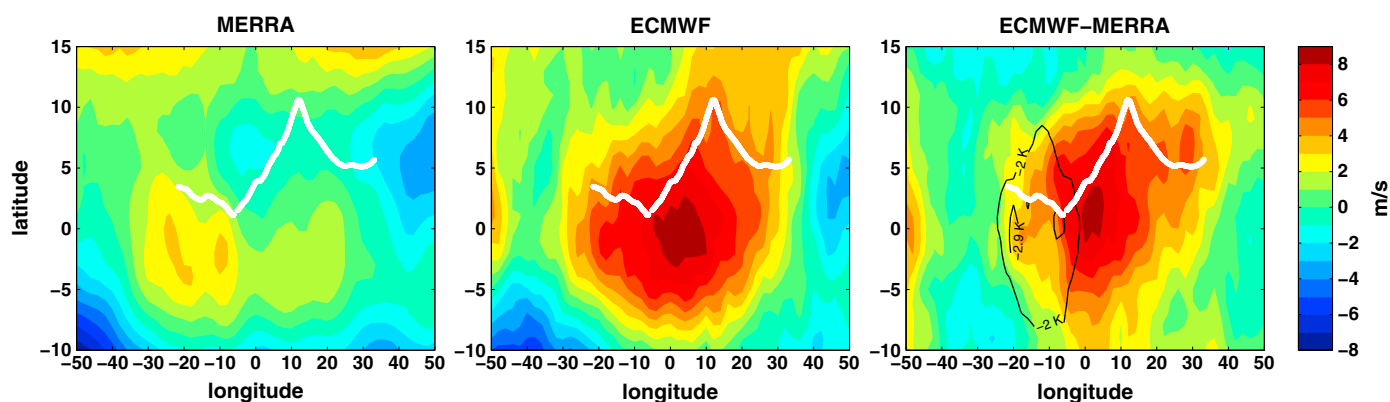


Figure 6. Composite maps of zonal wind perturbations in a frame moving at 20 m/s eastward in (left) MERRA, (middle) ECMWF operational analysis, and (right) the difference between those, at 61.5 hPa. These maps are obtained by temporally averaging the zonal wind fields shifted in longitude so that a point moving at 20 m/s eastward would keep the same longitude. Longitude 0 corresponds to longitude 10° on 5 April and to longitude 100° on 10 April. In Figure 6 (right), black contours are temperature differences between MERRA and ECMWF analysis. The white line corresponds to balloon 2 trajectory in the moving frame, in which the balloon drifts westward. The composite have been calculated during the first wave packet of case A (from 5 to 10 April).

deficiencies during this period. In particular, the difference between zonal mean zonal winds (i.e., the QBO) at 61.5 hPa in both analyses is small (about 1 m/s) and, in fact, results in stronger zonal mean zonal wind in MERRA.

Zonal wave number frequency spectra of zonal wind and temperature at the equator (not displayed) confirm that the difference between the two analyses stems from the representation of Kelvin wave packets. Total space-time variances are similar in both analyses for this period, but the spectral distributions significantly differ. Whereas ECMWF analysis exhibits more power in propagating disturbances (especially in the Kelvin wave modes with planetary wave numbers 3–4 and periods of 5–6 days), MERRA displays more stationary zonal wind and temperature features.

The previous discussion referred to the wind at the equator. Yet balloon 2 made excursions of a few degrees off the equator during the period corresponding to case A (see Figure 1). We now check whether the latitudinal structure of this Kelvin wave packet in ECMWF analyses is consistent with the persistent zonal wind positive perturbation observed in the balloon time series during these excursions. Figure 6 shows a composite map of zonal wind (color) and temperature (contours) in a frame moving eastward at 20 m/s to follow the propagation of the Kelvin wave packet (from 5 April to 10 April). Such a map isolates the wave packet structure in longitude-latitude. The white line represents the balloon 2 trajectory in the moving frame. It appears that the anomaly associated with the Kelvin wave packet extends up to 10° away from the equator, which is consistent with expectations from the linear theory as well as with studies of equatorial waves in reanalyses [Lott *et al.*, 2009]. The corresponding structure of the temperature difference between MERRA and ECMWF (black contours in Figure 6, right) is consistent with a Kelvin wave signature as well. The temperature discrepancy between MERRA and either the observations or the ECMWF analyses reaches ~3 K between 8 and 12 April.

This confirms that even when balloon 2 drifted away from the equator, it was still under the influence of a Kelvin wave packet that induces zonal wind disturbances 2 to 8 m/s higher in ECMWF analysis with respect to those in MERRA reanalysis. All these evidences therefore support the conclusion that the discrepancy between MERRA reanalyses and the balloon observations during case A comes from missing Kelvin wave packets in MERRA reanalysis.

4.2. Case B

Case B also shows differences between observed and analyzed zonal wind (Figures 1 and 4) on scales such that the QBO and equatorial waves are again the only possible processes whose misrepresentation can explain the observed discrepancy. However, in contrast with case A, ECMWF and MERRA both differ from the balloon observations so that we cannot use one of the analyses to understand the deficiencies of the other. Figure 2 recalls the dynamical context associated with case B in ECMWF operational analysis. It shows in

particular that the ECMWF analysis misses the dynamical process responsible for the eastward acceleration of the balloon around 10 March and lacks the eastward winds that are felt by the balloon after 25 March.

The first hypothesis thus consists in an inaccurate representation of the QBO in both reanalyses. During case B, balloon 1 was drifting at the level of maximum shear associated with the phase reversal of the QBO. The shear value in ECMWF analysis at that level is $-4 \text{ m s}^{-1} \text{ km}^{-1}$. With a mean apparent underestimation of the zonal velocity in the analyses of 8 m/s, the vertical shift of the QBO phase required to compensate for the wind deficiency would be of $\Delta z \approx -2 \text{ km}$, which looks unlikely high for a zonally homogeneous signal. Such a shift would correspond to three model levels in ECMWF operational analyses and two levels in MERRA reanalysis. Nevertheless, the 4–5 m/s difference at the end of case B (i.e., beginning of April) might be partly explained by invoking a misrepresentation of the QBO.

As for case A, the second hypothesis consists in a misrepresentation of equatorial waves in the analyses. During the 1 month time period associated with case B, the balloon drifted over half of the equatorial belt, and the long-standing discrepancy between the observed and analyzed winds is only seen in the zonal component. Therefore, it is again likely that the analysis deficiencies arise from the misrepresentation of planetary-scale Kelvin wave packets. Two further elements support this idea. First, the temperature variations recorded by the additional sensors on balloon 1 exhibit a 3 day long, positive temperature anomaly around 10 March, which is present in none of the analyses. This positive temperature perturbation before the zonal velocity counterpart is in agreement with the Lagrangian signature of an upward propagating Kelvin wave packet.

This is also supported by the structure of wind and potential temperature from radiosonde measurements at Singapore, which are displayed as vertical time diagrams in Figure 7 together with the winds from ECMWF analysis and their difference with those radiosonde observations. The height-time passage of balloon 1 at the longitude of Singapore is indicated by the black crosses. In agreement with the balloon time series, the radiosondes show that the balloon passage on 19 March occurred during a positive zonal velocity disturbance associated with one of these Kelvin wave packets. This 19 March wave packet clearly stands out in the ECMWF fields and the radiosondes (Figures 7a and 7b). However, the ECMWF operational analysis underestimates the amplitude of the Kelvin wave packet seen in the radiosounding data by about 8 m/s; this is a large difference, especially since the Singapore radiosondes are assimilated by ECMWF and the radiosonde observation errors are about 2–3 m/s. One likely reason for this large analysis error is the relatively short vertical wavelength of the observed wave packet, i.e., 2.5 km, which is not captured by ECMWF analyses, possibly because of the smoothing impact of the vertical structure functions in data assimilation, which can produce wave signals with lower amplitude and higher vertical scales than observed. Here dynamical arguments can explain the short vertical wavelength observed: indeed, the wave packet horizontal phase speed, estimated from its observed vertical wavelength and with the help of the dispersion relationship for Kelvin wave, is found to be around 15–18 m/s, i.e., near the time mean zonal mean zonal wind at that time and altitude. In other words, this Kelvin wave packet is close to a critical level.

Returning to the balloon and analysis time series (Figure 4), two further remarks should be made. First, although the Kelvin wave packet anomalies were underestimated by ECMWF analyses around 19 March, Figure 4 shows that this day and the following week correspond to a time period within case B when the differences between the analyzed and observed zonal winds are reduced. During this 1 week period, balloon 1 was drifting over the Maritime Continent (it crosses the date line on 24 March, 22:00 UT), whereas it was over the Indian Ocean before and over the central and eastern Pacific afterward. As for case A, this therefore suggests that the geographical distribution of dynamical observations in the TTL also plays a role in (the severity of) the analyses deficiencies.

The second remark concerns the apparent long-standing positive zonal wind anomaly in the balloon time series during case B and the absence of a negative counterpart. At first sight, this may be at odds with our interpretation in terms of a Kelvin wave packet, which is expected to induce both positive and negative anomalies. This paradox may, however, result from the eastward Stokes drift undergone by isopycnic balloons when they encounter a Kelvin wave. This is shown in detail in Appendix A1, where the Stokes drifts of isopycnic and isentropic tracers are contrasted. In particular, the balloon Stokes drift becomes larger when the Kelvin wave packet approaches a critical level, which seems to be the case here. Hence, the fact that the balloon spends longer times in the positive zonal wind anomalies (Stokes drift) and that the Kelvin

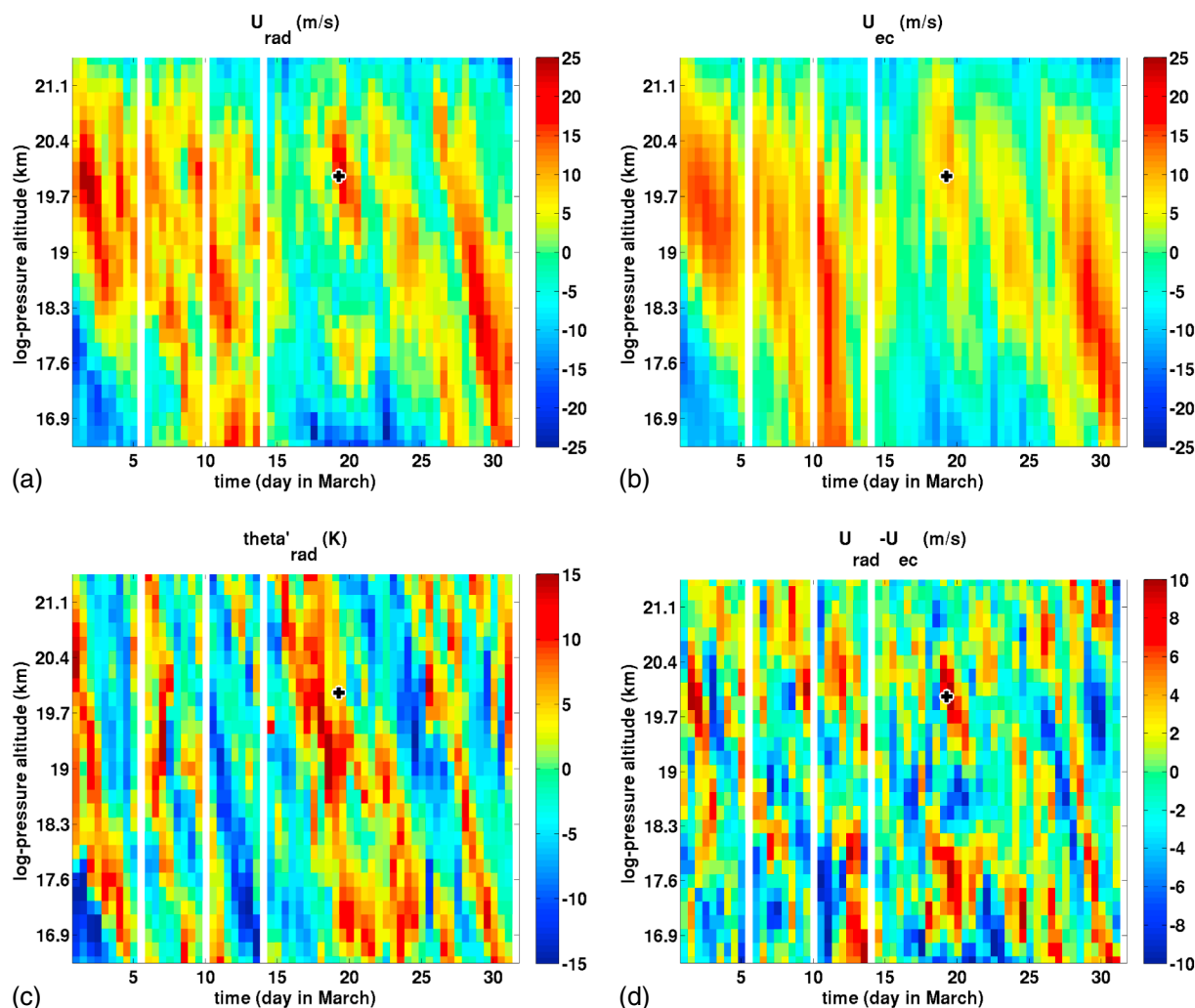


Figure 7. Log-pressure altitude-time diagrams of zonal wind from (a) radiosoundings measurements and (b) interpolated winds from ECMWF analysis, (d) of the difference between those and (c) of dry potential temperature anomalies with respect to the time average in March from radiosounding measurements at Singapore (104°E, 1.4°N). The black cross figures the time and altitude of the balloon when it crosses Singapore's longitude. The log-pressure altitude is related to pressure measurements through $z = H \ln \frac{P_0}{P}$ (where $H = 7$ km and $P_0 = 1000$ hPa), and the range displayed here corresponds to 45–95 hPa. Time resolution is that from the radiosoundings (twice a day at 0:00 and 12:00 UTC). Vertical resolution is the original for ECMWF analysis and of about 300 m (2.5 hPa) for radiosoundings (those data, originally about every 200 m, have been interpolated at constant pressure levels).

wave packets generally appear as a few (or even a single) oscillations (see, e.g., Figure 5) contributes to the observed prominence of positive zonal wind anomalies in the balloon time series.

4.3. Case C

During the period from 10 to 20 March, balloon 1 recorded oscillations of about 10 m/s in meridional wind that are absent or strongly underestimated by both the ECMWF operational analysis and MERRA reanalysis (case C; see Figures 1 and 4). This case is distinct from the previous ones because the missing oscillation appears mainly in the meridional wind rather than in the zonal wind and because it lasts for a shorter period of time. In addition, this error comes out as a missing oscillation rather than a negative bias.

The oscillations have a period of 3 to 4 days according to a wavelet analysis of the balloon time series. No such signal appears in the wavelet analysis of the zonal wind records, and the crossing of the equator by the balloons during that period is not associated with a 180° phase change of the meridional wind. The gravest equatorial wave corresponding to such a signature is the Yanai (or mixed Rossby-gravity) wave.

Yanai wave packets are a common feature of the equatorial stratosphere, especially in the positive phase of the QBO [Baldwin *et al.*, 2001]. They have been observed in many reanalysis products as well as in satellite

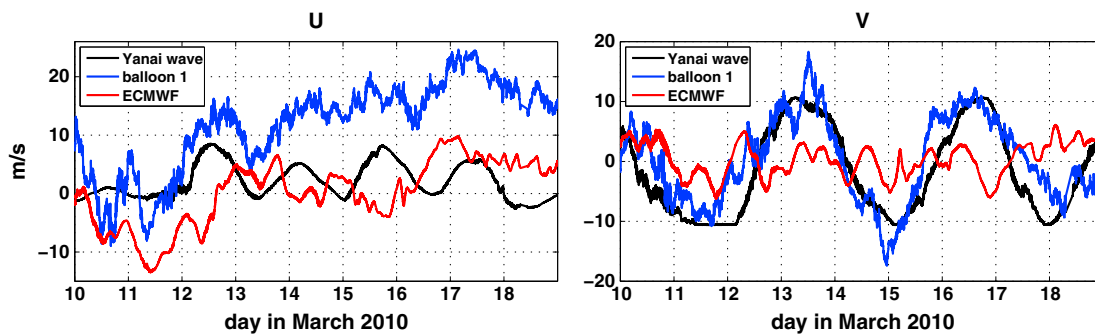


Figure 8. Time series of (left) zonal and (right) meridional wind along balloon 1 trajectory from observations, the ECMWF analysis, and from an idealized Yanai wave packet (see text for details).

and in situ observations of temperature and wind. *Vial et al.* [2001] also reported Yanai wave packet observation during a previous equatorial campaign of stratospheric balloons. The Hovmöller diagram of meridional wind in the ECMWF analysis (Figure 2) actually displays many instances of Yanai wave packets, and one of these is likely the cause of the meridional wind disturbances seen in the balloon 1 time series early in April (Figure 4). But no such signal appears either in ECMWF analyses or in MERRA reanalyses between 10 and 20 March.

As stressed by *Vial et al.* [2001], observations from one long-duration balloon only are not sufficient to completely characterize the wave: only its amplitude and its intrinsic frequency can be estimated. To further support that the disturbances seen in the observed winds (and lacking in the analyzed ones) are due to the lack of a Yanai waves in the analyses, we looked again at the radiosounding observations at Singapore, which show multiple passages of Yanai wave packets (not shown). In March 2010, Yanai wave packets in these radiosoundings typically have Eulerian periods of 5 to 5.5 days and vertical wavelengths of 3 to 3.5 km (which corresponds to planetary zonal wave number of 3–4) at ~ 60 hPa.

Figure 8 shows, together with the observed and analyzed wind time series during case C, reconstructed time series at the balloon position for an idealized Yanai wave on the equatorial β plane with properties similar to the packets observed in Singapore radiosoundings and with amplitude and phase based on balloon 1 observations. The short-scale fluctuations in the time series for the idealized Yanai wave come from interpolating at the positions of balloon 1. Most of the observed variability in the meridional wind (Figure 8, right) can be explained by this wave. In particular, the mean Lagrangian zonal velocity of the balloon is responsible for the difference between ground-based and intrinsic periods (3.5 versus 5 days). In the zonal wind time series (Figure 8, left), shown is a mean difference between the balloon time series and either the reconstructed or the ECMWF corresponding time series, which is due to the simultaneous presence of Kelvin wave activity (case B; see the previous section).

The reconstructed time series of the zonal wind (Figure 8, left) highlight two additional features. First, a signal with an amplitude of ~4 m/s and a doubled frequency compared to what is seen in the meridional wind appears in the reconstructed zonal wind time series. These Lagrangian oscillations seem to be in phase with similar oscillations in the zonal wind observations. The frequency doubling is associated with the antisymmetric structure about the equator of the Yanai wave disturbance in zonal wind [*Vial et al.*, 2001]. The Yanai wave furthermore induces a mean positive deviation of the zonal wind, i.e., a balloon Stokes drift \bar{u}^S . Close to the equator, the Stokes drift expression for an isopycnic balloon is (see Appendix A2)

$$\bar{u}^S = \frac{1}{2} \frac{\sqrt{m^2 + \frac{1}{4H^2}}}{N} v_0^2 \quad (1)$$

where H is the atmospheric scale height, N is the Brunt-Väisälä frequency, and v_0 and m respectively are the Yanai wave amplitude of the meridional wind disturbance and vertical wave number. In our case, this expression yields $\bar{u}^S \sim 4$ m/s, which is consistent with the reconstructed time series displayed in Figure 8. The absence of the Yanai wave packet (and hence of the associated Stokes drift when interpolating at the balloon positions) in the (re)analyses may contribute to the underestimation of zonal winds between 10 and 20 March discussed in section 4.2, although the balloon excursions away from the equator would tend to reduce this value.

We conclude this section by noting that as for the previous cases, case C occurs while balloon 1 was drifting over the Indian Ocean, i.e., a region of the Earth where in situ observations are very sparse. With no wind observations available for the assimilation, the presence of Yanai wave in the analysis can come from the model (i.e., the first-guess field) or from temperature observations with high vertical resolution (from GPS measurements for instance) and enough latitudinal sampling to catch the antisymmetric signature of the Yanai wave in temperature. In order to represent appropriately the wind field structure from indirect temperature observations, the data assimilation system would need an appropriate balance relationship in its background error term. Even in the case of a perfect model, the temporal component of 4-D var in the tropics is not efficient to retrieve wind structure from tropical temperature observations [Žagar *et al.*, 2004]. It has been shown in Žagar *et al.* [2004] that the presence of the balance relationship for the Yanai wave in the background error term has a significant impact on the structure of analysis increment close to the equator. To our knowledge, no data assimilation system at present is applying balance background error coupling based on the equatorial wave theory. Thus, the Yanai and Kelvin waves, unless present in the first guess, may remain unrepresented in the tropical analyses in spite of their large-scale structure.

4.4. Other Events

In the previous subsections, we focused on the most striking cases of disagreement between the observed and analyzed winds during the PreConcordiasi campaign. Nevertheless, other (shorter) periods of (smaller) disagreement are observed as well. For instance, analyses underestimate for a few days the zonal wind observed by balloon 1 at the end of February, which recalls the signature of missed Kelvin waves. In late March and early April, the Yanai wave disturbances seen in balloon 1 meridional wind records are significantly underestimated by the analyses, which nonetheless succeeded to capture the signal. A few days after, the analyses underestimate balloon 1 meridional wind for a few days and therefore miss its northward drift away from the equator. Last, the balloons also show influence of higher-order modes, likely equatorially trapped inertio-gravity waves. Although those phenomena are important for driving the QBO [e.g., Evan *et al.*, 2012], they are not expected to imply large deviations in the trajectories of air parcels because of their short periods, and we will not elaborate further on them.

5. Discussion

In the previous section, we have reported several events of equatorial wave packets that were poorly represented or absent in the state-of-the-art analyses during boreal spring 2010 and thus lead to important errors in the corresponding analyzed wind (and temperature). We further discuss here the key factors that could cause such analysis deficiencies in the equatorial lower stratosphere, as well as some associated issues: (i) Are such errors likely to happen frequently? and (ii) What is their impact on the calculation of air parcel trajectories?

5.1. Factors Influencing (Re)Analysis Accuracy

Several factors can be involved alone or together in the reported misrepresentation of stratospheric equatorial wave packets in the analyses: the (parameterized) physics and mean large-scale dynamics of the model, its resolution and of course limitations in the assimilation itself. We briefly discuss here those factors.

5.1.1. Model Physics and Dynamics

The model physics and the parameterization of convection are expected to have huge impacts on the generation of equatorial waves, which are driven by the global time-space structure of latent heat release associated with deep tropospheric convection [Bergman and Salby, 1994; Horinouchi *et al.*, 2003; Ortland *et al.*, 2011]. Different convection parameterizations are used at ECMWF and in MERRA, based on the Arakawa-Schubert [Arakawa and Schubert, 1974] and the Tiedtke [Tiedtke, 1989] convective schemes respectively. Recent studies have shown that despite significant improvements, these schemes produce time-space precipitation fields that exhibit several shortcomings when compared to state-of-the-art precipitation observations [Kidd *et al.*, 2013; Kim and Alexander, 2013b]. In particular, features as essential as the organization of tropical convection or its diurnal cycle are still not well reproduced by the models. Also, the vertical profile of diabatic heating, which is crucial to determine the excitation of equatorial waves, is poorly constrained by observations. Hence, it is possible that the waves generated internally by the models do not match the actual atmospheric waves (in terms of vertical scale, diurnal cycle...) and need adjustments by the assimilation system.

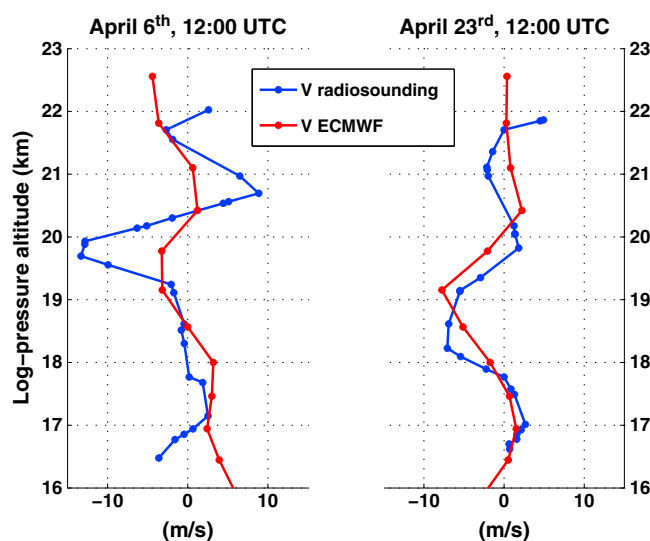


Figure 9. Vertical profiles of winds on 6 and 23 April, at Singapore (104°E, 1.4°N). In blue are the observed meridional wind profile from radiosoundings. In red are the meridional wind according to ECMWF analysis.

On top of a correct generation, equatorial waves must propagate through an analyzed TTL with realistic large-scale dynamics. Recently, *Flannaghan and Fueglistaler [2013]* have emphasized the importance of upper TTL winds (at pressure levels near 200 hPa) for the propagation of Kelvin wave packets. The background winds can cause wave breaking, convergence, or divergence of wave rays and hence induce significant Kelvin wave variability in the lower stratosphere. However, we found no illustration of such effects in the events reported here: for our case A, differences between MERRA and ECMWF mean TTL winds cannot explain the differences in stratospheric wave activity (the westward winds above the Indian Ocean in MERRA reanalysis would rather produce a convergence of Kelvin wave rays there).

5.1.2. Model Vertical Resolution

Vertical resolution is another well-known factor influencing equatorial wave representation in numerical models [e.g., *Boville and Randel, 1992*], and the three case studies we presented involved waves with vertical wavelengths smaller than 6 km. Indeed, even if the waves were properly generated and could propagate through a realistic background atmosphere, limited vertical resolution would damp the shortest ones more than they would be in the atmosphere. The assimilation of observation containing those waves would also prove difficult.

To illustrate this, Figure 9 displays vertical profiles of meridional winds measured by radiosondes at Singapore (light brown) on 6 and 23 April 2010, as well as the corresponding profiles in the ECMWF analysis (blue). On both dates, radiosonde data exhibit vertically oscillating structure in the meridional wind, which are likely associated with Yanai wave packets. On 23 April 2010, Yanai wave disturbances have a larger vertical wavelength (~ 4 km). Now the disturbances are more realistic in the ECMWF analyses on 23 March than on 6 March so that the model vertical resolution obviously plays a role in the accuracy with which analyses are able to reproduce planetary-scale features like Kelvin or Yanai waves. This may be due to the smoothing by the data assimilation procedure, which will be the strongest for vertical wavelengths that are short relative to the model's vertical resolution. This suggests that the model vertical resolution is probably still an important aspect that operational centers have to consider to improve the analysis accuracy in the equatorial UTLS. On the other hand, ERAI reanalyses performance is close to that of ECMWF operational analysis despite a coarser vertical resolution; there are five vertical levels between 100 and 40 hPa in ERAI instead of 10 in the operational model in 2010.

5.1.3. Geographic Distribution of Observations

As seen in Figure 1, the three cases we described happened when the balloons were over the Indian Ocean or the Eastern Pacific, regions where in situ observations are scarce. Figure 10 shows the overall longitudinal distribution of root-mean square (RMS) error in zonal wind (left) and temperature (right) for ECMWF analysis and MERRA reanalysis along the trajectories of the two PreConcordiasi equatorial balloons. Care must be taken with this representation since it is based on the measurement performed by two balloons only. Nevertheless, it stresses that wind RMS errors are almost twice as large over the Indian Ocean and eastern Pacific (nearly 8 m/s) as over regions with sounding stations, i.e., South America (60°–90° west) and the Maritime Continent (100°–150° east). This statement holds for both ECMWF and MERRA analyses, even if ECMWF shows overall better performances. It is also noteworthy that areas with weaker errors seem to extend to the east of regions with radiosoundings. This is probably because the assimilated information is advected

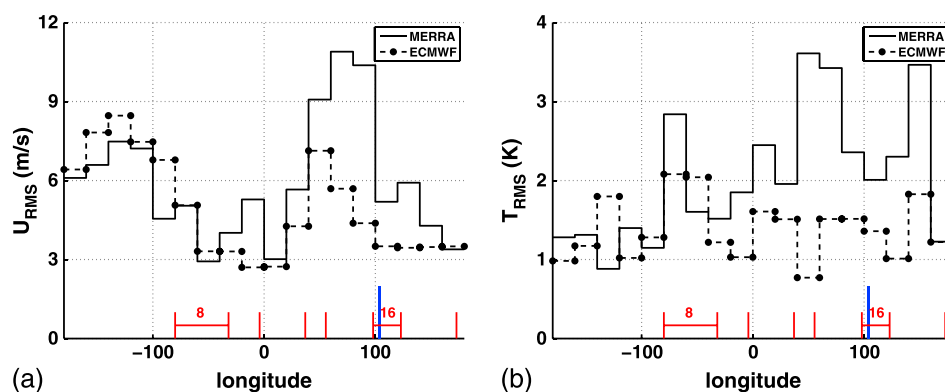


Figure 10. Root-mean-square error for (left) zonal wind (in m/s) and (right) temperature (in K) for MERRA (solid lines) and ECMWF analysis (dotted lines). For temperature, only the measurements of balloon 2 were used. Also shown are the longitudes of Singapore (blue line) and of other radiosounding stations (in red) located between 5° north and south (8 over South America and 16 over the Maritime Continent).

downstream of these regions by the prevalent eastward flow during the campaign. Moreover, Kelvin (and Yanai) wave packets propagate also eastward. This asymmetry in reanalysis errors with respect to continents has also been previously reported for the Southern Hemisphere stratosphere during the Eole campaign in the early 1970s [Hertzog *et al.*, 2006].

The longitudinal structure of analyses errors in temperature is quite different. Although MERRA still shows larger differences with the balloon observations over the Indian Ocean, the ECMWF analysis, which again performs better, shows a more uniform distribution along the equatorial belt. One key difference between ECMWF operational analyses (and ERAi reanalyses) and MERRA reanalyses is that ECMWF assimilated the refractivity profiles provided by the radio occultation of GPS signals. This additional data set, which is evenly distributed in longitude, may explain the reported differences in temperature between ECMWF and MERRA.

To extend our comparison beyond the two PreConcordiasi balloon trajectories, we also examined the structure of ECMWF analysis increments. Analysis increments for a variable x are defined as the difference between the analysis x_{an} and its first guess x_{fg} :

$$\delta x = x_{an} - x_{fg}. \tag{2}$$

Here we use the increments obtained as the difference between the 00 and 12 UTC ECMWF operational analyses and the corresponding 6 h forecasts respectively launched at 18 UTC and 6 UTC.

Figure 11 shows Hovmöller diagrams (bottom) of the analysis increments and the longitudinal structure of their time-averaged values (top). In addition, the time-averaged values of root-mean-squares (RMS, top) of the zonal (left) and meridional (middle) winds as well as temperature (right) are shown. All values are averaged between 5° south and 5° north on model level 33 (~65 hPa). The radiosounding station locations are also represented. The Hovmöller diagrams clearly show that analysis increments in wind components tend to be located in regions with radiosoundings, i.e., over South America (~70° west) and the Maritime Continent (~100° east). Consequently, significant time-averaged increments in the zonal wind analysis are found over these two regions, especially over South America. On the contrary, the time-averaged increments in the well-observed temperature field are small and do not exhibit a sharp zonal wind structure. Together with Figure 10, Figure 11 suggests that the errors in the analyzed winds in the deep tropics have a structure reversed relative to increments. The limited areas where corrections are available do not allow to fully constrain the flow over the equatorial belt, and increments are constantly needed to match assimilated observations where these exist. In short, for lower stratospheric winds in the tropics, the increments distribution is mostly determined by the distribution of wind observations. This has also been seen in data assimilation experiments [Horanyi *et al.*, 2013].

At the same time, the above also illustrates the inefficiency of data assimilation (including 4-D var and even a perfect model case) to extract information about circulation from dense temperature observations [Žagar *et al.*, 2004]. Although tropical stratospheric dynamics and its importance for global circulation are

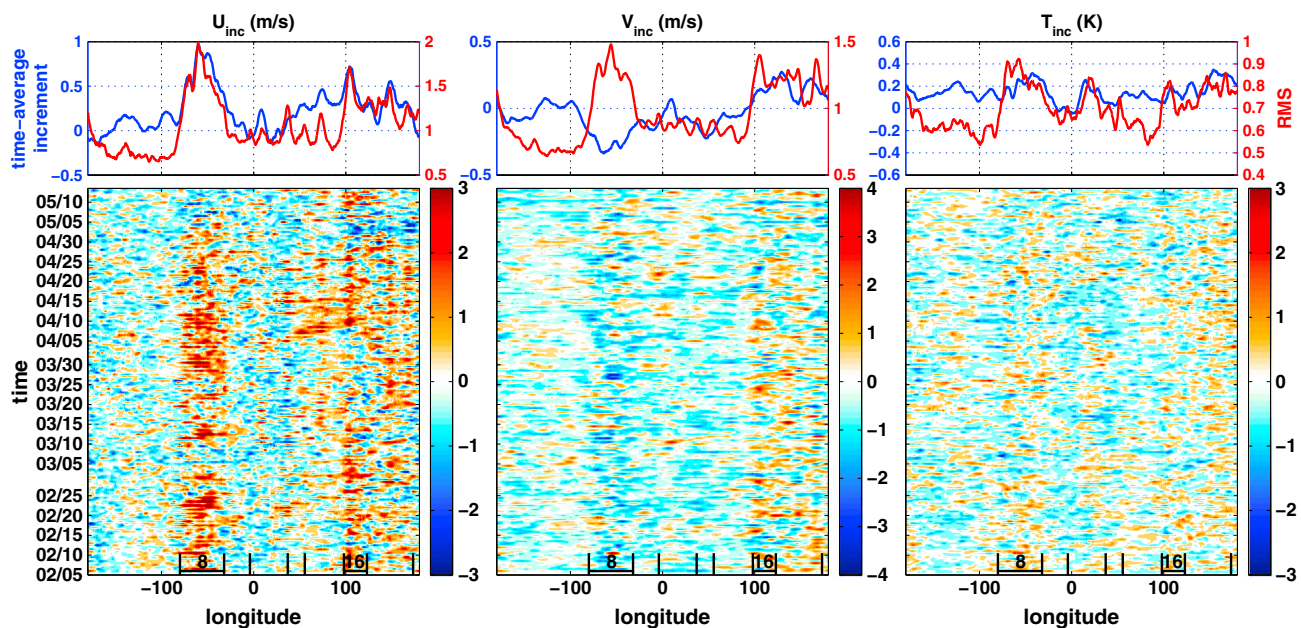


Figure 11. Longitudinal structure (top row) of the time-averaged increments (blue) and of their RMS (red) and (bottom row) Hovmöller diagrams of those increments for (left) zonal and (middle) meridional wind and (right) temperature, averaged between 5° north and 5° south, on ECMWF hybrid level 33 (about 65 hPa), in February–May 2010. In black, longitudinal locations of radiosondes between 5° north and south are represented at the bottom of the bottom row.

well understood, global data assimilation systems do not consider tropical waves in their balancing procedures. In spite of large advancements in the quality of tropical forecast and analyses in the last decade, the analysis increments here presented illustrate an important problem of the lack of direct wind observations [Baker et al., 2013]. Missions such as Atmospheric Dynamics Mission-Aeolus [Stoffelen et al., 2005] are therefore eagerly expected to fill the observation gap.

5.2. Error Frequency

The PreConcordiasi data set does not allow to monitor the seasonal or interannual evolution of analyses errors nor to follow the improvement of numerical weather prediction system over the years. Yet a few remarks can be made based on the dynamical characteristics of the cases reported here.

First, we note that the Kelvin wave events (especially case B) involved wave packets that were close to their breaking levels. In those cases, a comprehensive linear treatment suggests that the amplitude of equatorially trapped wave grows and that their vertical wavelength and latitudinal extent reduce [Lindzen, 1971]. This would obviously tend to render their assimilation more difficult.

Hence, we can speculate that analyses will miss Kelvin wave events more frequently during eastward shear phases of the QBO, while missed Yanai waves would be more likely during westward shear phases of the QBO. In all cases, strong shear phases are more likely to show critical levels for equatorial waves and would probably present stronger error events. Last, because of their weaker signature in temperature and shorter vertical wavelength in average, it is probably even more challenging for weather prediction systems to capture Yanai waves than Kelvin waves.

5.3. Consequences on Trajectory Calculations

Events of missed planetary equatorial waves like those reported here may have large impacts on air parcel trajectories computed with analyzed dynamical fields. To quantify this, we compared simulated balloon trajectories using the ECMWF operational analysis with the real trajectory of balloon 1. The trajectories were computed using a fourth-order Runge-Kutta scheme with an adaptive time step keeping the Courant number less than 1, having a default value of 15 min. For the calculations, analysis fields were interpolated in time and space using cubic splines. We calculated two sets of 40 isopycnic trajectories, lasting 10 days each and initialized from the balloon position every 6 h during two periods: from 11 to 21 February on the one

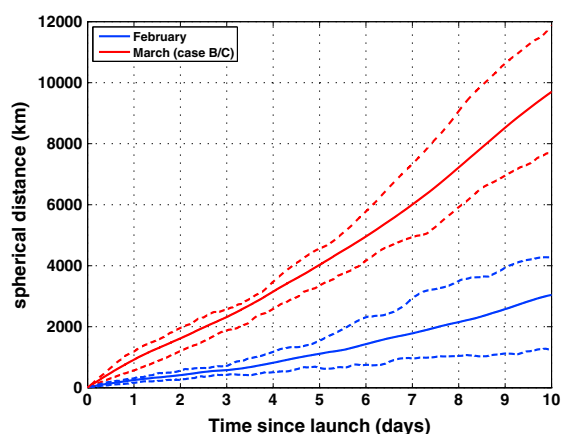


Figure 12. Spherical distance between balloon 1 positions and those deduced from balloon trajectory calculations in ECMWF operational analysis. (blue) Trajectories launched in mid-February 2010 when the observed and analyzed winds are in fair agreement and (red) trajectories launched in mid-March 2010 when planetary equatorial waves are missed by the analyses. Both statistics are based on forty 10 day trajectories. The solid line indicates the mean distance, while the dashed lines envelop 50% of the trajectories.

2010 are found to be significantly less accurate than above Antarctica in 2005 [Boccara *et al.*, 2008] or in the southern subtropics and midlatitudes flights in 2004 [Knudsen *et al.*, 2006], where mean separations of 500 km and 750 km after 5 days of simulation were respectively reported.

A recent work by Kim and Alexander [2013a] has emphasized the underestimation of equatorial waves in trajectory calculations based on reanalyses. Part of the underestimation comes from the interpolation between model levels, which reduces waves present in the analyses, and another part comes from the overall underestimation of equatorial waves in analyses. Kim and Alexander [2013a] have proposed a remedy for the former source of underestimation. Their methodology uses a Fourier transform in time to retain the equatorial waves that are present at model levels when interpolating between levels. Regarding the second source of underestimation, they proposed to amplify these high-frequency signals when one uses the analyzed fields to advect air parcel. Kim and Alexander focused on the effects of temperature anomalies, which are fairly well represented in reanalyses. Our study suggests that at least for the period studied, part of the analyses deficiencies is associated with equatorial wave packets that are essentially absent from the analyzed winds so that their method would not be sufficient to compensate for positional errors.

6. Summary and Conclusions

This paper presented an assessment of winds and temperature provided by ECMWF operational analysis as well as ERAi and MERRA reanalyses in the equatorial lower stratosphere (18–20 km, 15°S to 15°N). Those products were evaluated against in situ observations collected during long-duration stratospheric balloon flights between February and May 2010. Our main result is that the (re)analyses occasionally show very significant and persistent errors near the equator, especially in winds. For instance, ECMWF operational analysis exhibits errors as large as 8 m/s for 20% of balloon 1 flight duration (i.e., about 20 days), even though it shows the best performances among the data sets used in this study. Such errors are found to be much larger than at middle or high latitudes at the same altitude. The disagreements concentrate during well-defined periods that can last up to 20 days. During those periods, it was shown that advecting the balloon with the analyzed winds results in large errors on the balloon position, up to 10,000 km after 10 days of simulation. Our results therefore suggest that caution should be used when interpreting results based on long trajectories computed with analyzed winds at low latitudes.

An investigation of the error events shows that they primarily correspond to the large-scale equatorial waves missed by the analyses. It was shown that the assimilation system has greater difficulties in

hand and from 13 to 23 March on the other hand. The former period corresponds to a time interval when the observed and analyzed winds are in general agreement, while the latter corresponds to the beginning of cases B and C, where both Kelvin and Yanai waves were missed by the ECMWF analysis (Figure 4).

Figure 12 shows, for the two considered periods, time series of the average spherical distance between the positions of the real and simulated balloons, as a function of time since the launch of the simulated trajectories. As expected, the distance between the observed and simulated balloons grows much faster in March than in February. In March, the trajectory separation is impressive: during the first days, it increases almost linearly at a rate of 800 km/d and thus reaches 4000 km after only 5 days of simulation. For comparison, the separation between the observed and simulated balloons in February is of ~1000 km at that term, i.e., a factor 4 smaller. For both cases, the ECMWF-analyzed winds in the deep tropics in

representing the wave packets with a shorter vertical scale even over well-observed regions such as Indonesia. The analysis errors are probably enhanced when equatorial waves are near to critical levels and thus have small vertical wavelength and induce large disturbances in horizontal winds. But the main factor explaining the discrepancies between observed and analyzed winds appears to be the lack of direct observations of stratospheric wind profiles over wide regions along the equatorial belt. Analysis errors are the largest where observations are very scarce, in the eastern Pacific and Indian Ocean. In contrast, analysis increments are systematically largest in regions where observations are available.

Recently, ECMWF increased its vertical resolution from 91 to 137 vertical levels, which should improve the representation of waves with short vertical wavelengths in both forecasts and analyses. Yet TTL forecasts seemed hardly improved by this change [Bauer *et al.*, 2013]. New wind observations together with improved assimilation methodology, which would take into account the relations between temperature and winds in tropical waves, are the key for further improvements.

Appendix A: Balloon and Air Parcel Motion in Equatorial Wavefield

A1. Kelvin Wave

We here consider successively the trajectory of an isentropic air parcel and of a superpressure balloon in a monochromatic Kelvin wave. A perturbative calculation will reveal the presence, for the balloon, of a Stokes drift which can be of significant amplitude.

On short time scales (a few days), air parcels in the lower stratosphere behave almost isentropically. Embedded in a monochromatic Kelvin wave, the air parcel's position $(X(t), Z(t))$ verifies the equations

$$\frac{dX}{dt} = U \cos(kX + mZ - \omega t + \Phi_0)$$

$$\frac{dZ}{dt} = W \cos(kX + mZ - \omega t + \Phi_0 + \delta\Phi_0)$$

with U and W the amplitudes of the Kelvin wave in zonal and vertical winds. From the polarization relations we have

$$\delta\Phi_0 = 0, W = -\frac{k}{m}U.$$

In other words, the velocity perturbations associated to the wave are perpendicular to the wave number, as for internal gravity waves. This implies that

$$kX + mZ = cst.$$

In a Kelvin wavefield under Boussinesq approximation, the air parcel's positions describe segments in the x - z plane. Noting $\Phi = kX + mZ + \Phi_0 = cst$ we can write

$$u(X(t), Z(t), t) = -U \cos(-\omega t + \Phi).$$

Hence, there is no Stokes drift for an isentropic air parcel in a monochromatic Kelvin wave. In the presence of uniform background zonal wind \bar{u} , the change of variable $X' = X - \bar{u}t$ leads to the same result with ω replaced by $\hat{\omega} = \omega - k\bar{u}$.

Now superpressure balloons are not isentropic but isopycnic. In the Boussinesq approximation, the displacement of isopycnic surfaces relative to isentropic ones is

$$\zeta_p = \alpha \zeta_\theta \text{ with } \alpha = \frac{\frac{\partial \bar{T}}{\partial z} + \frac{g}{C_p}}{\frac{\partial \bar{T}}{\partial z} + \frac{g}{R}}.$$

α is always positive and inferior to unity in the stable atmosphere. In the lower stratosphere, we typically have

$$\frac{R}{C_p} = 0.285 < \alpha < 0.34.$$

The trajectory of a balloon may then be calculated as

$$\frac{dX_b}{dt} = U \cos(kX_b + mZ_b - \omega t + \Phi_0)$$

$$Z_b \text{ such that } \rho_{\text{air}}(X_b, Z_b, t) = \rho_b,$$

where the subscript b indicates a property (position and density) of the balloon.

The trajectory may be obtained perturbatively, assuming that the wave amplitude is small enough for the resulting displacements to be small relative to the wavelength ($U/\omega k \ll 1$). This hypothesis is justified given the scale of equatorial Kelvin waves. To leading order, the balloon undergoes oscillations around its initial position (X_b^0, Z_b^0) :

$$X_b^1 = -\frac{U}{\omega} \sin(kX_b^0 + mZ_b^0 - \omega t + \Phi_0) \quad (\text{A1})$$

$$Z_b^1 = \alpha \frac{kU}{m\omega} \sin(kX_b^0 + mZ_b^0 - \omega t + \Phi_0).$$

Injecting this in the right-hand side of equation (A1), one finds that there is a stationary contribution to the velocity at next order, namely, the Stokes drift:

$$\left\langle \frac{dX_b^2}{dt} \right\rangle = \bar{u}^S = \frac{1}{2} \frac{U^2}{\hat{c}} (1 - \alpha),$$

where the brackets $\langle \rangle$ denote time averaging, U is the amplitude of the Kelvin wave perturbation in zonal velocity, and $\hat{c} = \hat{\omega}/k$ is the phase speed. For waves close to their critical level and values similar to those found in the present study, the Stokes drift experienced by an isopycnic balloon can be significant (about 1.5 m/s for the Kelvin wave packet implied in case A and at least more than twice that number for case B).

A2. Yanai (or Mixed Rossby-Gravity) Wave

For the Yanai wave, the same kind of perturbative considerations and the use of the dispersion relation, namely,

$$\sqrt{m^2 + \frac{1}{4H^2}} = \frac{N}{\hat{\omega}^2} (\beta + \hat{\omega}k)$$

leads to the Stokes drift of an isentropic air parcel :

$$\bar{u}^S = \frac{1}{2} \frac{|M|}{N} \left(1 - \frac{2\beta|M|}{N} y^2\right) e^{-\frac{\beta|M|}{N} y^2} v_0^2$$

where v_0 is the amplitude of the meridional wind perturbation at the equator and $|M| = \sqrt{m^2 + \frac{1}{4H^2}}$. The isentropic Stokes drift is maximum at the equator and positive equatorward of $y = \pm \sqrt{\frac{N}{2\beta|M|}}$. The isopycnic equivalent has a similar but slightly different expression

$$\bar{u}^S = \frac{1}{2} \frac{|M|}{N} \left(1 - \frac{2\beta|M|}{N} y^2 + (1 - \alpha) \frac{\hat{\omega}^2}{N^2} |M|^2 y^2\right) e^{-\frac{\beta|M|}{N} y^2} v_0^2.$$

In these formulas, y stands for the average latitudinal position of the parcel or the balloon, which depends on their initial position y_0 and on the initial wave phase Ψ_0 , and is given at first order by

$$y = y_0 - \frac{V_0}{\hat{\omega}} \sin(\Psi_0).$$

Appendix B: Comparisons of Observations With the ERA Interim

The time series of winds in the ERA Interim, interpolated on the balloon trajectories, are displayed in Figure B1 together with the observations and results for other reanalyses. As mentioned earlier the results

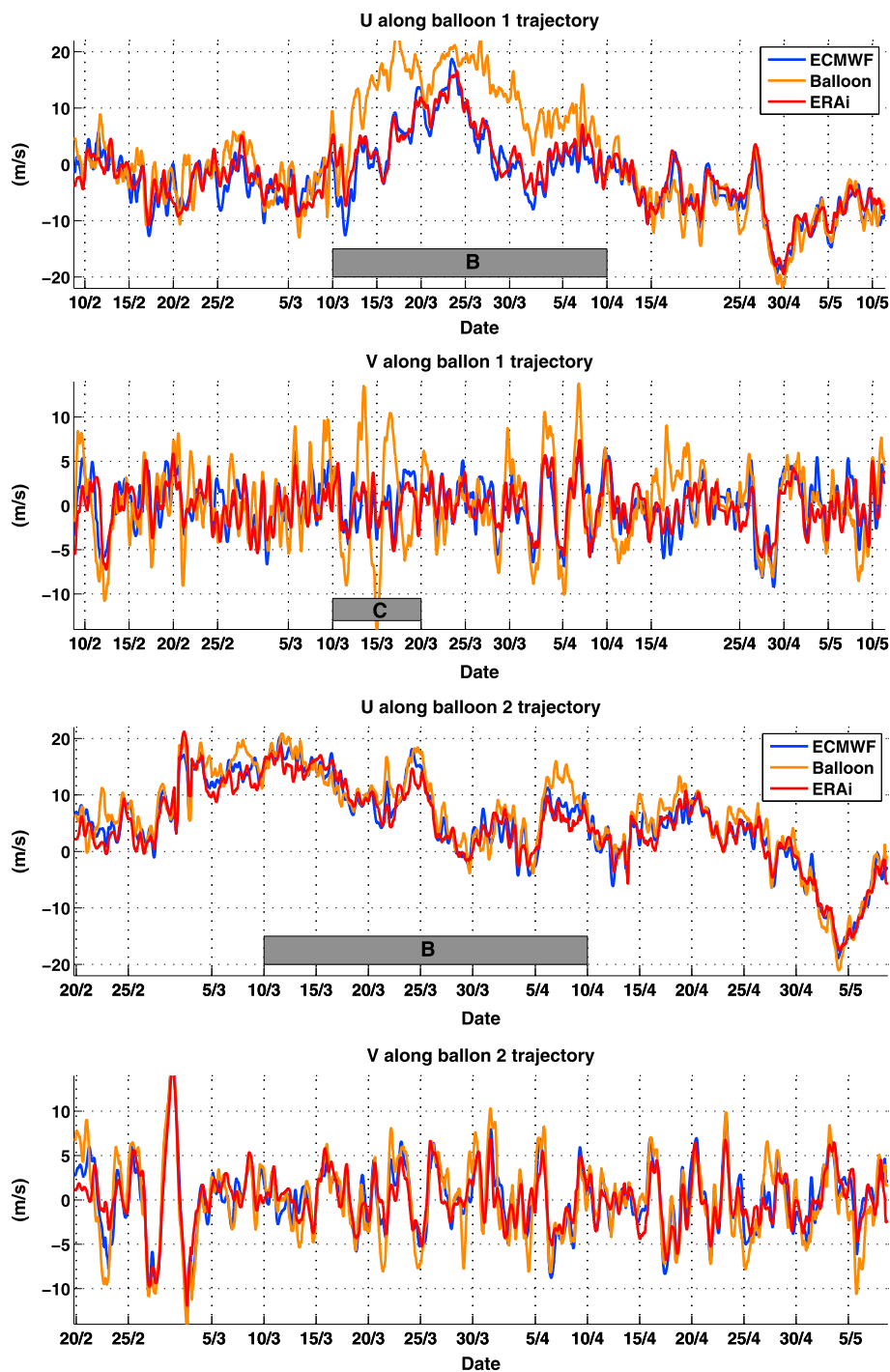


Figure B1. Time series of observed and analyzed winds from different analyses and reanalyses. Note the close results between the ECMWF operational analysis and the ERA Interim.

for ERA Interim are quite close to their equivalent in the ECMWF operational analysis, whereas there is almost a factor 2 in the number of vertical levels for those two analyses. However, both have about the same assimilated observations. This closeness suggests that the number of vertical levels is probably less critical than the quantity of assimilated observations.

Table B1 displays the correlation coefficients between wind observations and the three analyses. It confirms that the ECMWF operational analysis and ERA Interim are better compared to observations than MERRA.

Table B1. Correlation Coefficients Between Analyzed and Observed Winds

	<i>u</i>		<i>v</i>	
	Balloon 1	Balloon 2	Balloon 1	Balloon 2
MERRA	0.82	0.81	0.47	0.54
ECMWF	0.86	0.96	0.57	0.89
ERA Interim	0.87	0.94	0.53	0.79

Also, if the errors in meridional wind are less important than the ones in zonal wind, the corresponding analyzed times series are less correlated with observations. This is due to the smaller-scale, smaller-amplitude nature of meridional wind perturbations. They are mostly linked to mesoscale inertio-gravity

waves and small-scale gravity waves, which are poorly captured by the analyses but do not strongly influence trajectories.

Acknowledgments

PreConcordiasi balloon data used in this study can be found at <ftp://ftp.lmd.polytechnique.fr/hertzog/balloon/Pre-Concordiasi/tsen/>. The authors are grateful to Vincent Guidard, François Lott and Bernard Legras for fruitful discussions. A.P. acknowledges financial support from the Ecole Normale Supérieure. R.P., A.H., and A.P. acknowledge support from ANR project StrADyVariUS (Stratospheric Dynamics and Variability). N.Z. and A.H. would like to acknowledge the International Space Studies Institute (ISSI) in Bern, Switzerland, for hosting the "Atmospheric Gravity Waves in Global Climate Prediction and Weather Forecasting Applications" team meetings, during which we were able to elaborate part of this work. Research of N.Z. is supported by the funding from the European Research Council, Grant Agreement no. 280153. Concordiasi is an international project, currently supported by the following agencies: Météo-France, CNES, CNRS/INSU, NSF, NCAR, University of Wyoming, Purdue University, University of Colorado, the Alfred Wegener Institute, the Met Office, and ECMWF. Concordiasi also benefits from logistic or financial support of the operational polar agencies (Institut Polaire Français Paul Emile Victor) IPEV, Programma Nazionale di Ricerche in Antartide (PNRA), United States Antarctic Program (USAP) and (British Antarctic Survey) BAS, and from Baseline Surface Radiation Network (BSRN) measurements at Concordia. Concordiasi is part of The Observing System Research and Predictability Experiment International Polar Year (THORPEX-IPY) cluster within the International Polar Year effort. We thank Joan Alexander and two anonymous reviewers for their comments that helped to improve the paper.

References

- Anthes, R. A., et al. (2008), The COSMIC/FORMOSAT-3 mission: Early results, *Bull. Am. Meteorol. Soc.*, *12*(6), 313–333, doi:10.1175/BAMS-89-3-313.
- Arakawa, A., and W. Schubert (1974), Interaction of a cumulus cloud ensemble with the large-scale environment. Part 1, *J. Atmos. Sci.*, *31*, 674–701, doi:10.1175/1520-0469(1974)031<0674:IOACCE>2.0.CO;2.
- Baker, W. E., et al. (2013), Lidar-measured wind profiles: The missing link in the global observing system, *Bull. Am. Meteorol. Soc.*, *94*, 543–564, doi:10.1175/BAMS-D-12-00164.1.
- Baldwin, M. P., et al. (2001), The quasi-biennial oscillation, *Rev. Geophys.*, *39*, 179–229.
- Bauer, P., E. Andersson, and D. Richardson (2013), New model cycle 38r2, *ECMWF Newsletter*, *136*, 8–8.
- Bechtold, P. M., M. Koehler, T. Jung, F. Doblas-Reyes, M. Leutbecher, M. J. Rodwell, F. Vitart, and G. Balsamo (2008), Advances in simulating atmospheric variability with the ECMWF model: From synoptic to decadal time-scales, *Q. J. R. Meteorol. Soc.*, *134*, 1337–1351.
- Bergman, J. W., and M. L. Salby (1994), Equatorial wave activity derived from fluctuations in observed convection, *J. Atmos. Sci.*, *51*(24), 3791–3806.
- Boccara, G., A. Hertzog, C. Basdevant, and F. Vial (2008), Accuracy of NCEP/NCAR reanalyses and ECMWF analyses in the lower stratosphere over Antarctica in 2005, *J. Geophys. Res.*, *113*, D20115, doi:10.1029/2008JD010116.
- Boehm, M., and J. Verlinde (2000), Stratospheric influence on upper tropospheric tropical cirrus, *Geophys. Res. Lett.*, *27*, 3209–3212.
- Boville, B. A., and W. J. Randel (1992), Equatorial waves in a stratospheric GCM: Effects of vertical resolution, *J. Atmos. Sci.*, *49*, 785–801.
- Dee, D. P., et al. (2011), The ERA-Interim reanalysis: Configuration and performance of the data assimilation system, *Q. J. R. Meteorol. Soc.*, *137*(656), 553–597, doi:10.1002/qj.828.
- Dinh, T., D. R. Durran, and T. Ackerman (2012), Cirrus and water vapor transport in the tropical tropopause layer: Part 1—A specific case modeling study, *Atmos. Chem. Phys.*, *12*(20), 9799–9815, doi:10.5194/acp-12-9799-2012.
- Ern, M., P. Preusse, M. Krebsbach, M. G. Mlynczak, and J. M. Russell III (2008), Equatorial wave analysis from SABER and ECMWF temperatures, *Atmos. Chem. Phys.*, *8*(4), 845–869, doi:10.5194/acp-8-845-2008.
- Evan, S., M. J. Alexander, and J. Dudhia (2012), WRF simulations of convectively generated gravity waves in opposite QBO phases, *J. Geophys. Res.*, *117*, D12117, doi:10.1029/2011JD017302.
- Flannaghan, T. J., and S. Fueglistaler (2012), Tracking Kelvin waves from the equatorial troposphere into the stratosphere, *J. Geophys. Res.*, *117*, D21108, doi:10.1029/2012JD017448.
- Flannaghan, T. J., and S. Fueglistaler (2013), The importance of the tropical tropopause layer for equatorial Kelvin wave propagation, *J. Geophys. Res. Atmos.*, *118*, 5160–5175, doi:10.1002/jgrd.50418.
- Fueglistaler, S., and Q. Fu (2006), Impact of clouds on radiative heating rates in the tropical lower stratosphere, *J. Geophys. Res.*, *111*, D23202, doi:10.1029/2006JD007273.
- Fueglistaler, S., M. Bonazzola, P. H. Haynes, and T. Peter (2005), Stratospheric water vapor predicted from the Lagrangian temperature history of air entering the stratosphere in the tropics, *J. Geophys. Res.*, *110*, D08107, doi:10.1029/2004JD005516.
- Fueglistaler, S., A. E. Dessler, T. J. Dunkerton, I. Folkins, Q. Fu, and P. W. Mote (2009), Tropical tropopause layer, *Rev. Geophys.*, *47*(1), RG1004, doi:10.1029/2008RG000267.
- Hasebe, F., et al. (2013), Cold trap dehydration in the tropical tropopause layer characterised by SOWER chilled-mirror hygrometer network data in the Tropical Pacific, *Atmos. Chem. Phys.*, *13*, 4393–4411, doi:10.5194/acp-13-4393-2013.
- Hertzog, A., C. Basdevant, F. Vial, and C. R. Mechoso (2004), The accuracy of stratospheric analyses in the Northern Hemisphere inferred from long-duration balloon flights, *Q. J. R. Meteorol. Soc.*, *130*, 607–626.
- Hertzog, A., C. Basdevant, and F. Vial (2006), An assessment of ECMWF and NCEP-NCAR reanalyses in the Southern Hemisphere at the end of the pre-satellite era: Results from the EOLE experiment (1971–72), *Mon. Weather Rev.*, *134*, 3367–3383.
- Hertzog, A., et al. (2007), Strateole/Vorcore: Long-duration, superpressure balloons to study the Antarctic lower stratosphere during the 2005 winter, *J. Atmos. Oceanic Technol.*, *24*(12), 2048–2061, doi:10.1175/2007JTECHA948.1.
- Horanyi, A., M. Rennie, and L. Isaksen (2013), The expected NWP impact of Aeolus wind observations, *ECMWF Newsletter*, *137*, 23–29.
- Horinouchi, T., et al. (2003), Tropical cumulus convection and upward-propagating waves in middle-atmospheric GCMs, *J. Atmos. Sci.*, *60*(22), 2765–2782, doi:10.1175/1520-0469(2003)060<2765:TCCAUV>2.0.CO;2.
- Kawatani, Y., S. Watanabe, K. Sato, T. J. Dunkerton, S. Miyahara, and M. Takahashi (2010), The roles of equatorial trapped waves and internal inertia-gravity waves in driving the quasi-biennial oscillation. Part I: Zonal mean wave forcing, *J. Atmos. Sci.*, *67*, 963–980, doi:10.1175/2009JAS3222.1.
- Kidd, C., E. Dawkins, and G. Huffman (2013), Comparison of precipitation derived from the ECMWF operational forecast model and satellite precipitation datasets, *J. Hydrometeorol.*, *14*, 1463–1482, doi:10.1175/JHM-D-12-0182.1.
- Kim, J.-E., and M. Alexander (2013a), A new wave scheme for trajectory simulations of stratospheric water vapor, *Geophys. Res. Lett.*, *40*, 5286–5290, doi:10.1002/grl.50963.
- Kim, J.-E., and M. J. Alexander (2013b), Tropical precipitation variability and convectively coupled equatorial waves on submonthly timescales in reanalyses and TRMM, *J. Clim.*, *26*, 3013–3030, doi:10.1175/JCLI-D-12-00353.1.

- Knudsen, B. M., T. Christensen, A. Hertzog, A. Deme, F. Vial, and J.-P. Pommereau (2006), Accuracy of analyzed temperatures, winds and trajectories in the Southern Hemisphere tropical and midlatitude stratosphere as compared to long-duration balloon flights, *Atmos. Chem. Phys.*, *6*, 5391–5397.
- Lindzen, R. (1971), Equatorial planetary waves in shear, *J. Atmos. Sci.*, *28*, 609–622.
- Liu, Y. S., S. Fueglistaler, and P. H. Haynes (2010), Advection-condensation paradigm for stratospheric water vapor, *J. Geophys. Res.*, *115*, D24307, doi:10.1029/2010JD014352.
- Lott, F., J. Kuttippurath, and F. Vial (2009), A climatology of the gravest waves in the equatorial lower and middle stratosphere: Method and comparison between the Era-40 re-analysis and the LMDz-GCM, *J. Atmos. Sci.*, *66*, 1327–1346.
- Massman, W. J. (1978), On the nature of vertical oscillations of constant volume balloons, *J. Appl. Meteorol.*, *17*, 1351–1356.
- Matsuno, T. (1966), Quasi-geostrophic motions in the equatorial area, *J. Meteorol. Soc. Jpn.*, *44*, 25–43.
- Ortland, D. A., M. J. Alexander, and A. W. Grimsdel (2011), On the wave spectrum generated by tropical heating, *J. Atmos. Sci.*, *68*, 2042–2060, doi:10.1175/2011JAS3718.1.
- Rabier, F., et al. (2010), The Concordiasi project in Antarctica, *Bull. Am. Meteorol. Soc.*, *91*(1), 69–86, doi:10.1175/2009BAMS2764.1.
- Reverdy, M., V. Noel, H. Chepfer, and B. Legras (2012), On the origin of subvisible cirrus clouds in the tropical upper troposphere, *Atmos. Chem. Phys.*, *12*(6), 14,875–14,926, doi:10.5194/acpd-12-14875-2012.
- Rienecker, M. M., et al. (2011), MERRA: NASA's Modern-Era Retrospective Analysis for Research and Applications, *J. Clim.*, *24*, 3624–3648, doi:10.1175/JCLI-D-11-00015.1.
- Schoeberl, M. R., A. E. Dessler, and T. Wang (2012), Simulation of stratospheric water vapor and trends using three reanalyses, *Atmos. Chem. Phys.*, *12*, 6475–6487, doi:10.5194/acp-12-6475-2012.
- Stoffelen, A., et al. (2005), The atmospheric dynamics mission for global wind field measurement, *Bull. Am. Meteorol. Soc.*, *86*, 73–87, doi:10.1175/BAMS-86-1-73.
- Suzuki, J., M. Fujiwara, T. Nishizawa, R. Shirooka, K. Yoneyama, M. Katsumata, I. Matsui, and N. Sugimoto (2013), The occurrence of cirrus clouds associated with eastward propagating equatorial $n=0$ inertio-gravity and Kelvin waves in November 2011 during the CINDY2011/DYNAMO campaign, *J. Geophys. Res. Atmos.*, *118*, 12,941–12,947, doi:10.1002/2013JD019960.
- Tiedtke, M. (1989), A comprehensive mass flux scheme for cumulus parameterization in large-scale models, *Mon. Weather Rev.*, *117*, 1779–1800, doi:10.1175/1520-0493(1989)117<1779:ACMFSF>2.0.CO;2.
- Vial, F., A. Hertzog, C. R. Mechoso, C. Basdevant, P. Cocquerez, V. Dubourg, and F. Nouel (2001), A study of the dynamics of the equatorial lower stratosphere by use of ultra-long-duration balloons: 1. Planetary scales, *J. Geophys. Res.*, *106*(D19), 22,725–22,743, doi:10.1029/2000JD000241.
- Žagar, N., N. Gustafsson, and E. Källén (2004), Variational data assimilation in the tropics: The impact of a background error constraint, *Q. J. R. Meteorol. Soc.*, *130*, 103–125.
- Žagar, N., J. Tribbia, J. L. Anderson, and K. Raeder (2009), Uncertainties of estimates of inertio-gravity energy in the atmosphere. Part II: large-scale equatorial waves, *Mon. Weather Rev.*, *137*, 3858–3873.
- Žagar, N., L. Isaksen, D. Tan, and J. Tribbia (2013), Balance and flow-dependency of background-error variances in the ECMWF 4D-Var ensemble, *Q. J. R. Meteorol. Soc.*, *139*, 1229–1238, doi:10.1002/qj.2033..
- Wheeler, M., and G. T. Kiladis (1999), Convectively coupled equatorial waves: Analysis of clouds and temperature in the wavenumber-frequency domain, *J. Atmos. Sci.*, *56*, 374–399, doi:10.1175/1520-0469(1999)056<0374:CCEWAO>2.0.CO;2.
- Yanai, M., and T. Maruyama (1966), Stratospheric wave disturbances in the tropical stratosphere, *J. Meteorol. Soc. Jpn.*, *44*, 291–294.